Online Monitoring of Solvent and Acid Gas Concentration in a CO_2 Absorption Process using Monoethanolamine

A.C. van Eckeveld

Master of Science Thesis

TU Delft Delft University of Technology

Process & Energy department

The Enel carbon capture pilot plant at Brindisi, Italy, is depicted at the cover page. The picture was taken from http://www.portotolleproject.com

Online Monitoring of Solvent and Acid Gas Concentration in a CO_2 Absorption Process using Monoethanolamine

Master of Science Thesis

For the degree of Master of Science in Mechanical Engineering
Delft University of Technology

Andries Cornelis van Eckeveld

October 23, 2013

Faculty of Mechanical, Maritime and Materials Engineering (3mE)
Delft University of Technology

Delft University of Technology
Department of Process & Energy
Faculty ofMechanical, Maritime and Materials Engineering (3mE)

The undersigned hereby certify that they have read and recommend to the Faculty of Mechanical, Maritime and Materials Engineering for acceptance a thesis entitled

Online Monitoring of Solvent and Acid Gas Concentration in a CO_2 Absorption Process using Monoethanolamine

by

A.C. van Eckeveld

in partial fulfillment of the requirements for the degree of

Master of Science Mechanical Engineering

Dated: October 23, 2013

Supervisors:

Prof.dr.ir. B.J. Boersma	Dr.ir. L.V. van der Ham

Examination committee:

Prof.dr.ir. B.J. Boersma	Dr.ir. L.V. van der Ham
Dr.ir. C. Poelma	Dr.ir. H.J.M. Kramer
	Dr.ir. L.F.G. Geers

Acknowledgements

First, I would like to thank my day-to-day supervisor Leen van der Ham for his support and assistance during this project. His sharp analysis, questions and useful suggestions supported me during the development of this thesis work.

My sincere thanks go to prof. Bendiks Jan Boersma for his support from the TU Delft and for his supervision and criticism along the way. My thanks go to all other colleagues from TNO for being opens to my question and helping me out, especially with experimental issues concerning the mini- and microplant and the other experimental work I have performed. And of course for the 'gezelligheid' during lunches and borrels and at the coffee machine.

I am very thankful to TNO in general and particularly to the former research manager of the Gas Treatment department, Sven van der Gijp, for giving me the opportunity to do my master thesis there and for all facilities I was able to use.

Finally, I want to thank my family and friends for supporting me during my studies and particularly during this project and for being interested in the work I carried out at TNO.

Delft, October 23, 2013 A.C. van Eckeveld

Abstract

Enhanced greenhouse gas emisions in the past century contributed to the global average temperature rise. The emission of greenhouse gases, therefore, should be limited in the coming decades. One way to do so is by capturing the greenhouse gasses (like CO_2) from industrial flue gases (post-combustion capture). This can be achieved in a chemical absorption process using monoethanolamine as a solvent.

In this report, the development of a method has been developed for the real-time liquid analysis of the solvent and absorbed acid gas concentrations in a post-combustion capture process using monoethanolamine as a solvent, capturing CO_2. Online monitoring of the dynamic behaviour of these process properties is of major importance from a process control and a scientific perspective. Currently this is only achieved using fourier transfrom infrared spectroscopy, combined with a multivariate calibration method called chemometrics. This is, however, an expensive method and there are limitations with respect to robustness and actual process installation. The developed method is based on cheap and easy measurable properties of the solvent. Inverse Least-Squares models were built at two temperature levels, based on a set of 29 lab-prepared samples with different MEA and CO_2 concentrations. Density, conductivity, refractive index and sonic speed measurements were used as input data in model development since this combination of quantities showed the best performance with respect to predictive accuracy and apparatus costs of all assessed analytical techniques.

The developed model has been validated during continuous operation of a mini CO_2 capture plant. The concentrations of MEA and CO_2 were predicted with a mean error of 0.53 and 0.31 [wt%] for MEA and CO_2 respectively. Process dynamics, like step-changes in the CO_2 flue gas concentration, were covered accurately as well. The model showed good robustness to changes in solvent temperature.

Robustness of the model against solvent degradation was assessed using samples from the TNO pilot plant at the Maasvlakte and during a three week experiment at a microplant. First some degraded samples were added to the model calibration set for improved robustness purposes. Both the polluted model and the unpolluted model were able to monitor the MEA and CO_2 concentrations of the pilot plant samples and in the microplant accurately. The addition of degraded samples to the calibration set did improve the predictive accuracy of the model if the degradation products in the monitored process were of the same nature as the degradation products that were added to the calibration set. The combination of the model with process data has shortly been assessed, but further study in this direction is required.

Combining density, conductivity, refractive index and sonic speed measurements with a multivariate chemometric method enables the real-time and accurate monitoring of the acid gas and monoethanolamine concentrations in CO_2 absorption processes, even under degrading process conditions.

Table of Contents

List of Figures

List of Tables

Chapter 1

Introduction

1-1 Carbon capture

The earth's mean temperature has risen gradually over the last 50 years and there is a growing consensus amongst climate researchers about the contribution of human activities to this temperature rise[1]. Industrialization has led to enhanced emissions of greenhouse gases into the earth's atmosphere, contributing to global warming. Many greenhouse gases have been identified and water vapour and carbon dioxide are considered to be the most important ones, the latter of which is mainly emitted from industries using fossil fuels as a primary energy source[2].

Although fossil fuels will eventually be replaced by renewables, for the coming decades they will remain as the major energy source for society and industry. One way to reduce the carbon footprint of men during the transition to renewables is Carbon Capture and Storage (CCS). CCS is the process of capturing CO_2 from large point sources, such as fossil fuel power plants, and subsequent transportation and storage at dedicated storage sites. A schematic representation of the CCS chain is given in Figure 1-1.

Since the power and industry sector account for more than 60% of the world's CO_2 emissions[4], capturing CO_2 from industrial flue gases has a great potential to reduce the emission of this major greenhouse gas into the atmosphere[5]. The International Energy Agency (IEA) estimated that 17% of the total CO_2 emission reductions in 2050 will be achieved by CCS as is depicted in Figure 1-2. Furthermore, the costs per tonne mitigated CO_2 emission by CCS is less compared to e.g. offshore wind and photovoltaic technologies[6].

Different CCS technologies are currently being studied and the most well-known amongst these technologies are pre-combustion capture, post-combustion capture and oxy-fuel com-

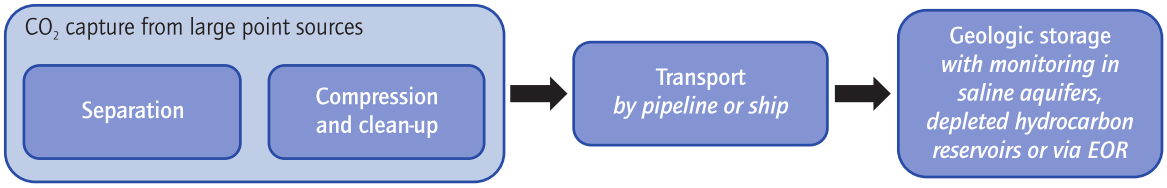

Figure 1-1: Schematic representation of the CCS chain [3]

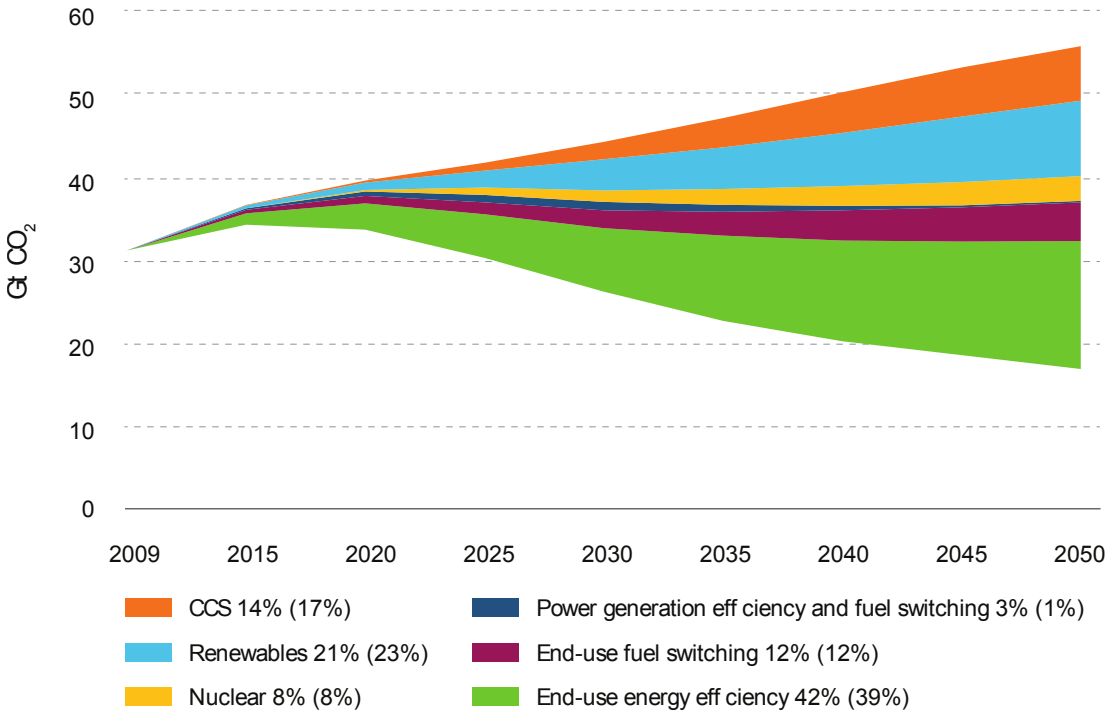

Figure 1-2: Potential energy-related CO_2 emission reductions by technology [6]. Percentages represent the share of the cumulative emission reduction through 2050, bracketed values represent the share of reductions in the year 2050.

bustion. In pre-combustion capture, the fossil fuel is partially oxidized and the CO_2 is captured from the resulting syngas, before it is combusted. The CO_2 concentration and partial pressure in the syngas is high compared to typical flue gases, enabling a more efficient capture step. Pre-combustion capture is considered to be the most mature among the different capture technologies, since it is the only technique that is currently applied at a full scale power plant (Kemper County IGCC) and it is the most chosen technology in planned projects worldwide at the moment[6]. It is, however, only applicable for new-build plants since large alterations in the fuel processing are required for existing conventional plants. For existing plants, Post-Combustion Capture (PCC) has the highest potential of becoming commercial in the coming decades. In PCC, the CO_2 is captured from the industrial flue gases after combustion. It typically uses a reactive solvent to absorb the acid gas from the entering flue gases. Alkanolamines are widely used as a solvent, with Monoethanolamine (MEA) being the most common[7]. The third CCS technology is oxy-fuel combustion, in which the fuel is burned with only oxygen instead of air. This results in flue gases consisting of mainly CO_2 and water vapour, which are easily separated by condensing the water vapour. The initial air separation step in which pure O_2 is obtained, however, demands a lot of energy and the increased flue gas temperature due to the combustion with solely oxygen, requires the use of special materials. A general, schematic representation of the described technical options for CCS is given in Figure 1-3.

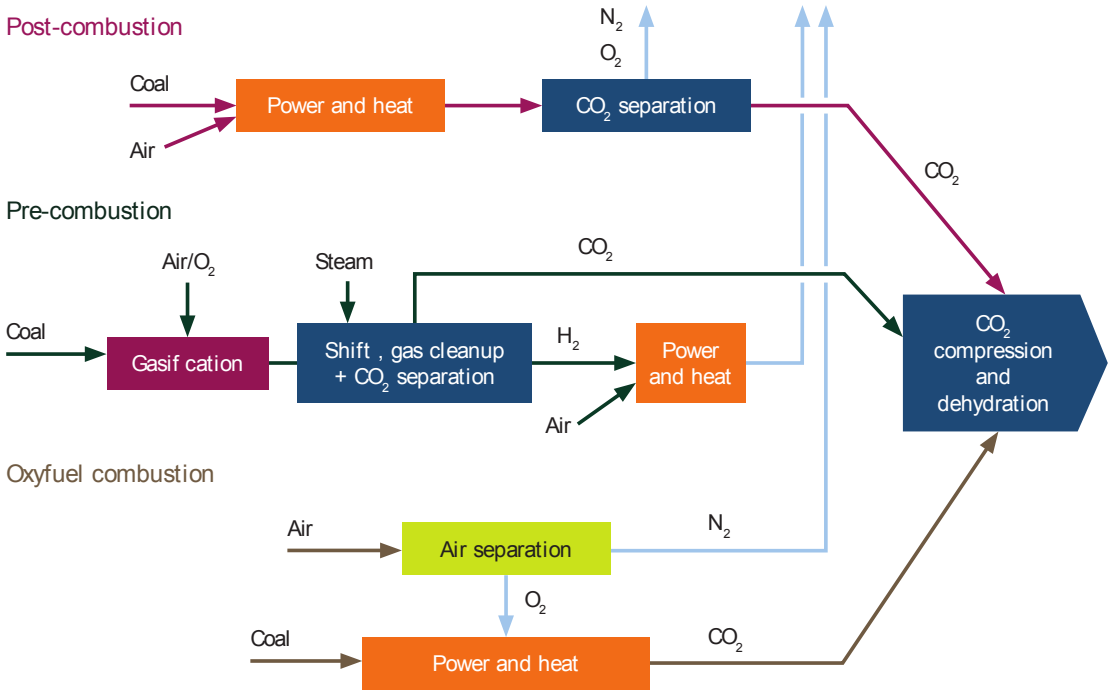

Figure 1-3: Technical CCS options for CO_2 capture from coal-fired power plants [6]

1-2 Post-Combustion Capture

In PCC processes the CO_2 is captured from flue gases produced by the combustion of fossil fuels. PCC has several advantages over the other CCS technologies, especially if it is retrofitted to existing plants. No large changes have to be made in process plants for PCC to be applicable. Currently, there are three main PCC processes: chemical absorption, adsorption and membrane separation[6]. In absorption processes, CO_2 is absorbed in a solvent, which is regenerated at elevated temperature and pressure. Adsorption is the process in which CO_2 is captured by a solid material and in membrane separation, a membrane is used to selectively permeate CO_2 from the flue gas. The latter two technologies have some advantages over chemical absorption (e.g. the lower energy requirement) but are nowadays still in development and only applied at small scale. Hence, PCC using chemical absorption is currently the most viable CO_2 capturing technology for retrofitting to existing industrial plants.

Although the PCC process is not very complicated (for a more detailed description refer to Section 2-1), controlling it is not an easy task. First, the flue gas composition and flow rate vary due to upstream operational variations in the (power) plant. Moreover, elevated temperatures and contamination of the flue gas cause solvent degradation and deactivation (Section 2-2). Controlling the process performance requires accurate monitoring of the amine solution in real-time. Two important parameters of the solvent that need to be monitored are the solvent concentration and the CO_2 loading. Nowadays, these parameters are measured by means of laboratory analysis of solvent samples, which is both time-consuming and laborious and therefore not applicable for direct operational purposes.

Attempts have been made to make use of fourier transform infrared (FTIR) in combination

with a multivariate analysis method (known as chemometrics) for real-time measurement of solvent concentration and acid gas loading and the results were promising as it comes to the accuracy of the predictions[8, 9]. There are, however, some disadvantages in using FTIR involving costs of the apparatus and need for it to be located within a few meters of the process. Furthermore, the method showed unsatisfactory results when the solvent mixture exceeds calibration limits for the different components or when it contains components the model was not properly calibrated for.

A more cost-effective method for determination of solvent and solute composition in the liquid can be found in the combination of easy measurable solvent properties with a multivariate chemometric method. Previously, some work has been done using different analytical techniques to determine the solvent composition. Conductivity measurements have been used for CO_2 concentration monitoring[10, 11], but the use of one analytical technique restricts the possible prediction to only one component. A combination of density and refractive index measurements has been evaluated for estimation of the solvent and solute concentrations in amine based CO_2 capture processes[12] and the results were promising in terms of predictive accuracy. However, the robustness of this technique to disturbances is limited due to the inclusion of only two measured quantities. The sensitivity of sonic speed to amine concentration was identified by Hawrylak et al.[13] and sonic speed might therefore be applicable for the prediction of the amine concentration in the solvent. Recently, a screening study has been carried out to assess the sensitivities of different simple analytical techniques to compositional changes in the solvent mixture[14]. Assessed solvent properties were conductivity, pH, density, refractive index and UV-vis spectra. Combinations of density, refractive index, conductivity and pH showed promising results for predicting the MEA and CO_2 concentrations of solvent samples. No method has been reported in literature concerning the online prediction of solvent composition, which is both cost effective and readily implemented.

1-3 Objectives

The objective of this study is to develop an empirical, chemometric model to monitor the performance of a PCC chemical absorption process in real time, based on easy measurable properties of the active solution and using a PCC process with MEA as active solvent as a base case. The following sub-goals are formulated:

1. Assess the suitability of different measurable solvent properties for determination of the MEA and CO_2 concentration in the solvent
2. Develop a chemometric model to determine the MEA and CO_2 concentration from the chosen analytical techniques
3. Validate the model performance both offline and online
4. Assess the robustness of the predictive performance of the model to solvent degradation

1-4 Approach

This study aims at the development of a method for online prediction of the solvent and solute concentration in a MEA-based PCC chemical absorption process. First several solvent properties have been assessed for their sensitivity to changes in the MEA and CO_2 concentrations in the solvent. Based on the results of these sensitivity experiments a selection of different properties is used for model calibration. For that purpose a calibration data set has been obtained by measuring the respective properties in prepared lab samples. Different combinations of measurements from that calibration set were used for model development and the best performing combination of properties, in terms of costs and predictive accuracy, was subsequently selected and used to calibrate a chemometric model. Validation of the model was done using both offline lab-sample measurements and online validation on a mini-pilot plant. The model robustness to solvent degradation was evaluated during a three-week continuous experiment, carried out at a microplant. Finally attempts were made to combine the model with process data.

1-5 Outline of the report

In Chapter 2 the theoretical background of this study is shortly described, both for MEA-based PCC and for chemometrics. Chapter 3 describes the experimental techniques that were used. The fourth chapter contains a manuscript on the model development and validation, that has been submitted to Industrial & Engineering Chemistry Research (IECR). The assessment of model robustness with respect to solvent degradation is covered in Chapter 5 and the process data attempts in Chapter 6. Conclusions and a future outlook are provided in Chapter 7.

Chapter 2

Theoretical background

2-1 Chemical absorption using MEA as solvent

Chemical absorption based on amine solvents is a very mature technique in capturing CO_2 and has been used ever since the 1930s in the process industry. Alkanolamines, chemical structures that carry an hydroxy and amino structure on a alkane basis, are common solvents in these kind of processes. They remove CO_2 from the entering gas stream by means of an exothermic reaction between the amine and the CO_2. Different amines have been investigated with respect to CO_2 capture capacity, stability and reactivity. The alkanolamines can be divided into three major groups: primary, secondary and tertiary amines, referring to the number of amine groups per molecule. In this study, a primary amine called Monoethanolamine (MEA) was used as a base case. It is the least expensive and it is known to have a high reactivity and hence can capture large quantities of CO_2 in a relatively short amount of time[15]. The drawbacks are that its capacity for CO_2 (on a molar basis) is low compared to secondary and tertiary amines, that the energy required for regeneration is relatively high and that it is sensitive to degradation from contaminants in the flue gas[7]. Notwithstanding these disadvantages, MEA has been used for over 70 years in the process industry and it has been researched widely as a reactive solvent in acid gas capturing processes.

The Post-Combustion Capture (PCC) process using chemical absorption with an amine-based solvent consists typically of an absorber column in which the flue gases contact the solvent in countercurrent. The acid gas is absorbed by the solvent and the cleaned flue gases leave the top of the absorber. The rich solvent (high CO_2 content) is then pre-heated in the lean-rich heat exchanger and fed to the stripper column, where the solvent is regenerated at elevated temperature and pressure. The operating temperature of the stripper is most often between 100 and 120 [°C] whereas the pressure is typically around 1.9 [bara]. In order to regenerate the solvent elevated temperatures are required. Too high temperatures, however, accelerate solvent degradation. The heat required to release the CO_2 from the solvent is supplied by a reboiler, often integrated with the steam cycle of the host plant. Steam and CO_2 are leaving through the top of the stripper and the steam is subsequently condensed from the CO_2, yielding a relatively pure CO_2 stream. The lean solvent (low CO_2 content) is leaving the bottom of the stripper column and exchanges heat with the rich solvent entering the stripper, before it enters the absorber again. A schematic representation of the process is provided in Figure 2-1.

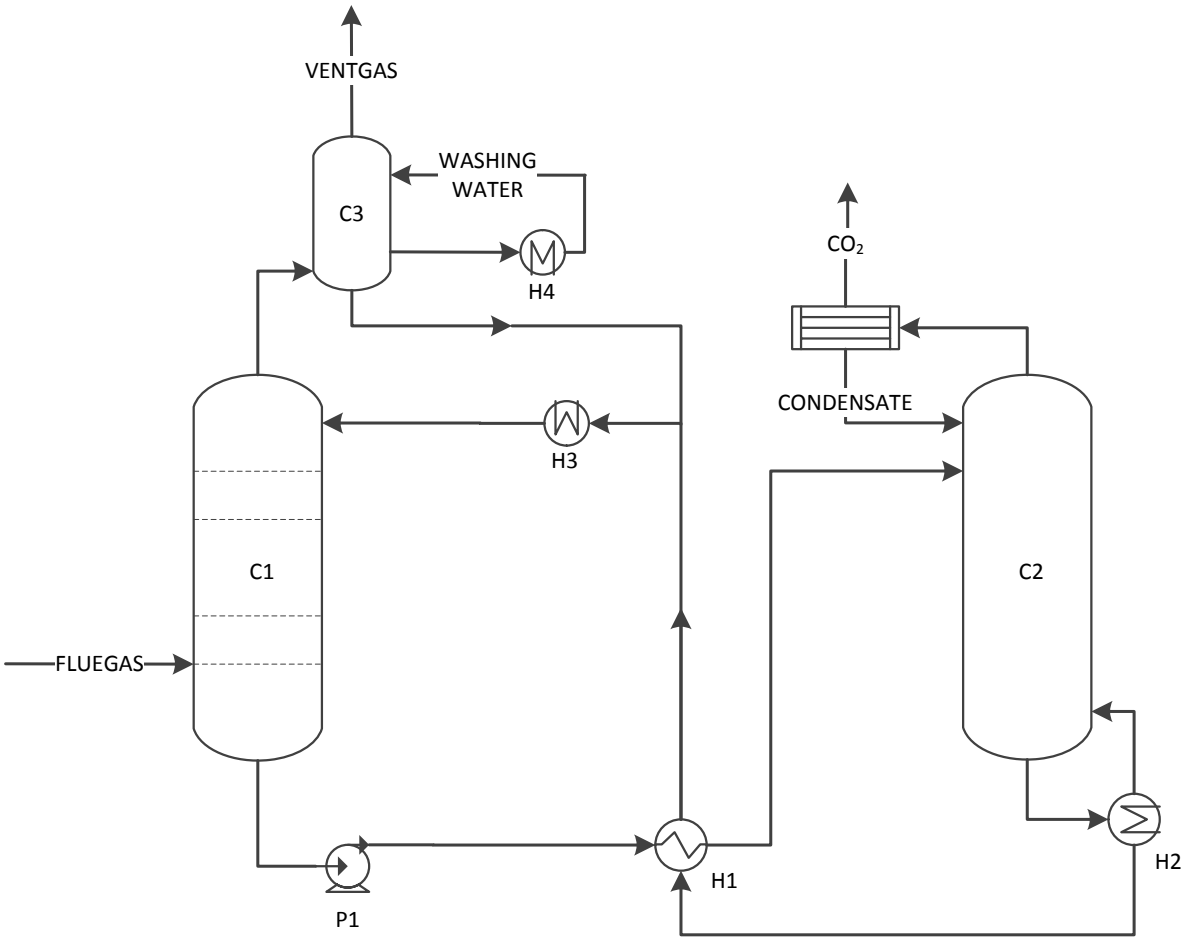

Figure 2-1: General flowscheme of PCC plant

The used solvent (MEA) is one of the simplest alkanolamines and consists of an ethanol molecule with an amine group opposite to the hydroxyl group:

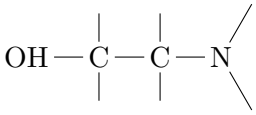

Figure 2-2: Monoethanolamine molecule

MEA is typically diluted to around 30 [wt%] in water to limit the solvent degradation (which increases at higher MEA concentrations) but to retain a significant CO_2 capturing capacity. The overall reaction between CO_2 and the aqueous MEA solution is usually represented as[16]:

$$CO_2 + MEA \rightleftharpoons MEACOOH \tag{2-1}$$

$$MEACOOH + MEA \rightleftharpoons MEACOO^- + MEA^+ \tag{2-2}$$

These reactions are reversed in the stripper. Reaction (2-1) is rate determining since Reaction (2-2) is considered to be an instantaneous reaction. The theoretically maximal CO_2 molar loading following from this reaction scheme is 0.5 mole CO_2 per mole MEA.

2-2 MEA degradation

The process performance depends not only on the MEA concentration and acid gas loading. The solvent degrades due to irreversible reactions with several components to form undesirable compounds, diminishing the absorbing capacity of the solvent. A disadvantage of using MEA as absorbent is the relatively high degradation rate due to reactions with e.g. SO_x, NO_x and O_2. The flue gasses should therefore be pre-treated to remove amine degrading contaminants. H_2S has to be removed as well since MEA favours its absorption over carbon dioxide. A complete removal of these contaminants is not feasible and degradation due to contamination has to be taken into account.

There is still some uncertainty about the actual degradation mechanisms for MEA, but the mechanisms can be classified in three different types: carbamate polymerization, oxidative degradation and thermal degradation of the solvent[17]. The latter requires temperatures over 200°C and will not occur under normal process conditions. The other two are treated in some more detail in this section. The formation of Heat Stable Salts (HSS) from MEA is covered as well.

Important for this study are the degradation products since they might disturb the developed model and are to be included in the screening experiments.

2-2-1 Carbamate polymerization

Carbamate polymerization occurs at elevated temperatures and in the presence of CO_2 (e.g. in the stripper). Under stripper conditions, Reactions (2-1) and (2-2) are reversed, but in some cases unwanted side reactions occur.

Polderman and Steel proposed a mechanism for carbamate polymerization of MEA that is widely accepted. The first step is the cyclization of MEA carbamate to 2-oxazolidone as is shown below[18].

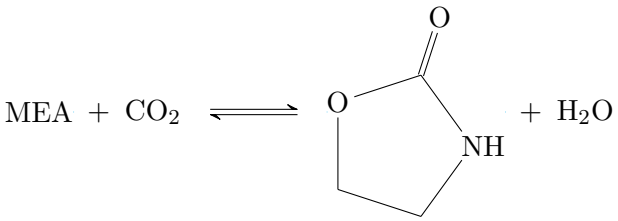

2-oxazolidone can further react irreversibly with free MEA to form 1-(2-hydroxyethyl)-2-imidazolidone, often referred to as HEIA.

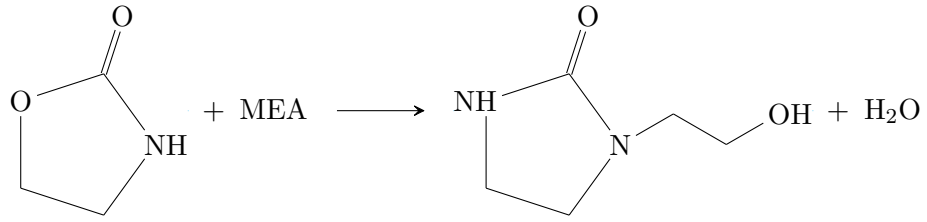

HEIA can subsequently be hydrolyzed to form N-(2-hydroxyethyl)-ethylenediamine, also known as HEEDA.

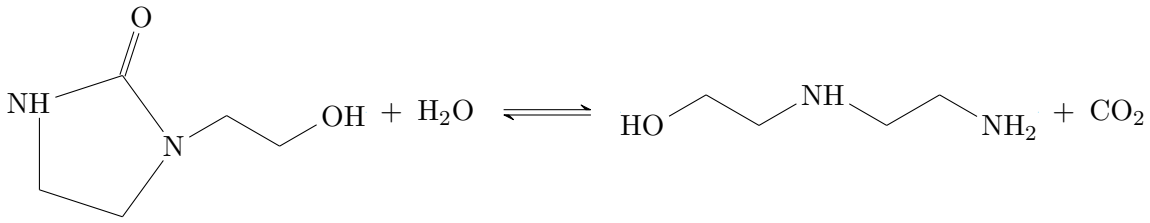

Yazvikova and Zelenskaya [19] discovered that an intermediate product is formed in the reaction of 2-oxazolidone to HEIA:

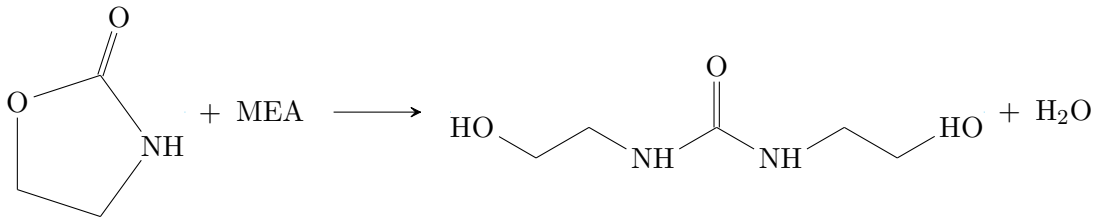

The product of this reaction, N,N'-di(2-hydroxyethyl)urea (DHU) converts to HEIA upon heating.

The production of HEIA appears to be the dominant phenomenon[20], with HEEDA playing a smaller role. HEEDA and HEIA are considered as key degradation components in carbamate polymerization. DHU is expected to play a minor role since it is an intermediate product in the formation of HEIA and it will therefore not accumulate in the process.

The kinetics of carbamate polymerization are positively depending on the MEA concentration, the CO_2 loading and the temperature, with the latter having the strongest influence.

For the screening experiments, HEIA is chosen as the representative component for carbamate polymerization since it is considered to be one of the most important products of this degradation process.

2-2-2 Oxidative degradation

Under oxidative conditions, MEA can degrade to various degradation products. The oxidation is driven by the presence of oxygen in the treated gas, leading to free radical reactions in the process. Dissolved iron, often present due to oxidation of the process equipment, plays a major role in the oxidation process because it catalyzes oxidation by decomposing peroxides into free radicals. Dissolved copper and nitrogen oxides are also catalysts for the oxidative degradation process.

Several pathways for the different oxidative degradation products have been proposed [17, 21]. The main observed degradation products include ammonia and organic acids such as acetic acid, formic acid, glycolic acid and oxalic acid[22]. Oxalic acid is found to be decomposing to formic acid, whereas the other acids react with MEA to form either imides or HSSs, the latter of which will be covered in the next section.

A pollutant mix has been included in the screening experiments, consisting of 5 oxidative degradation products: ammonia, formaldehyde, formic acid, acetic acid and oxalic acid.

2-2-3 Heat stable salts formation

HSSs are formed by the reaction of the amine solvent with strong acids. The oxidative degradation products of MEA, described in Section 2-2-2, are a well-known source of HSSs. Another source is the reaction of MEA with pollutants like hydrochloric acid (HCl), sulfuroxides (SO_x) and nitrogenoxides (NO_x) resulting in the formation of different salts (e.g. chloride, sulfate, nitrate), thereby reducing the active MEA concentration. These salts do not contribute to CO_2 capture, are not regenerated under normal process conditions and can, in high concentrations, damage the equipment due to their corrosive nature.

Common HSSs in amine processes include formate, acetate, oxalate, nitrate, nitrite, sulfate, sulfite and thiosulfate, the concentrations of which are depending on the contaminants present in the system. Nitrate, nitrite, sulfate, sulfite and thiosulfate originate from the presence of NO_x and SO_x in the flue gas while the other HSSs are formed from MEA degradation products.

HNO_3 and H_2SO_4 have been added to the samples as representative products from solvent contamination with NO_x and SO_x. These components and a part of the components in the pollutant mix, are also known to form HSSs with MEA.

2-3 Chemometrics

In this study, a model has been developed for the prediction of both MEA and CO_2 concentrations in the solvent. Chemometrics were used to calibrate and develop the model using experimentally obtained calibration data. Chemometrics is the application of statistical methods in chemistry[23, 24, 25]. Svante Wold was the first to introduce chemometrics to the world in an application in 1971 (see [26]). In the current study, chemometrics were used to solve a predictive problem (as opposed to a descriptive problem): properties of the chemical system were modeled to predict new properties of interest. Chemometrics were both used in multivariate calibration of the developed model and in data compression by means of Principal Component Analysis (PCA) and Partial Least Squares (PLS). In this section a short introduction into chemometrics and data handling is provided.

2-3-1 Scaling

The raw measurement data was pretreated to remove (part of) the noise and to be able to compare different measurements with each other. The main pre-treatment methods are shortly described in this section.

Mean-centering involves the subtraction of the average response of each variable from all responses of that variable (Equation(2-3)). This operation removes unwanted leverage effects from the data, to focus on the differences in the data induced by changes in Y-variables (or predicted variables, as opposed to X- or measured variables). Both X- and Y-data is usually mean-centered.

$$\mathbf{X}_{mc} = \mathbf{X} - \mathbf{1}_N \cdot \bar{\mathbf{x}} \tag{2-3}$$

Variance scaling, on the other hand, involves division of the data by the standard deviation of the responses in the respective variable (Equation 2-4). Variance scaling is mainly important if responses from different measurement techniques are compared. It prevents the variables with the largest absolute range to dominate the other variables. A data set is said to be z-scored if both mean-centering and variance scaling are applied.

$$\mathbf{X}_{z-scored} = (\mathbf{X} - \mathbf{1}_N \cdot \bar{\mathbf{x}})(diag(\mathbf{S}))^{-1} \tag{2-4}$$

It is sometimes desirable to scale a block (a number of variables of the same type) using the same scaling factor. Blockscaling is warranted if a data set contains different "blocks" of the same type of variables, e.g. the wavelengths in spectroscopic data.

Pretreatment techniques for spectroscopic data

Spectroscopic data is characterized by the large number of X-variables (or wavelengths) that are simultaneously measured. Besides the previously described block-scaling, special pretreatment techniques have been developed for this kind of data.

Windowing is the most straightforward preprocessing technique for spectroscopic data. It is aimed at selecting the relevant variables (or wavelengths) that are affected by the species of interest. Although this technique can easily be implemented, it is a very rough filtering technique. There is a risk of throwing away relevant data and of increasing the influence of noise on the data.

Baseline drift and differences in baseline slope of the spectroscopic data can be removed making use of derivatives of the data set. The first derivative of the data removes the baseline drift and the second derivative also removes baseline slope from the data. This can be needed in comparing peaks in measured spectra.

Multiplicative Scatter Correction (MSC), Standard Normal Variate (SNV) and Orthogonal Signal Correction (OSC) are examples of pretreatment techniques that have been effectively used in many spectroscopic applications, mainly in near infrared (NIR) spectroscopy. MSC and SNV are techniques to correct for light scattering and reflectance in sample response profiles[27]. OSC filtering is aimed at removing (spectral) variations that are unrelated to changes in sample composition. The use of OSC filtered data leads in general to a less complex and more robust final model.

2-3-2 Chemometric techniques

Numerous different chemometric methods have been developed, each having its own advantages and disadvantages. Depending on the size, the noise level, the non-linearity and other characteristics of the data set, a proper method has to be applied. The most important and well-known chemometric methods that can be used in model development are covered in this section.

Classical least squares

Classical Least Squares (CLS) is one of the simplest and most straightforward chemometric techniques and can be considered a starting point for other, more sophisticated methods. It is a direct classical expression of the absorbance version of the Lambert-Beer law (Equation 3-10) for a multiple analytes system:

$$\mathbf{X} = \mathbf{Y}\hat{\mathbf{K}} + \mathbf{E} \tag{2-5}$$

In case of the Lambert-Beer law, $\mathbf{K}$ represents the pure component spectra of the species present. The estimator of these spectra ($\hat{\mathbf{K}}$) is found from Equation (2-6) and using that estimator, the concentrations of all analytes are assessed.

$$\hat{\mathbf{K}} = (\mathbf{Y}^t\mathbf{Y})^{-1}\mathbf{Y}^t\mathbf{X} \tag{2-6}$$

$$\hat{\mathbf{Y}}_{unk} = \mathbf{X}_{meas}\hat{\mathbf{K}}(\hat{\mathbf{K}}\hat{\mathbf{K}}^t)^{-1} \tag{2-7}$$

There are some drawbacks in using CLS and one of the most important restrictions is that all analytes that are present in the mixture must be known. In other words, the concentration of all components in all calibration samples is required. Furthermore, the model becomes unstable if there is a substantial amount of collinearity between the responses for different analytes. In addition, CLS presumes perfect linearity between dependent and independent variables which, most often, does not reflect reality. CLS also requires to have at least as many samples (m) and variables (n) as there are analytes and hence large calibration sets are needed if many analytes are present.

CLS is a very simple and straightforward method that, if all restrictions are fulfilled, yields reasonable results with a relatively small effort.

Inversed Least Squares

As implied by its name, the Inversed Least Squares (ILS) method is the inverse of the CLS method:

$$\mathbf{Y} = \hat{\mathbf{B}}\mathbf{X} + \mathbf{E} \tag{2-8}$$

It therefore, in contrast with CLS, assumes that the error is included in the concentrations (dependent or Y-variables) rather than in the measurements (independent or X-variables). The calibration matrix $\hat{\mathbf{B}}$ is found using Equation (2-9).

$$\hat{\mathbf{B}} = \mathbf{Y}\mathbf{X}^t(\mathbf{X}\mathbf{X}^t)^{-1} \tag{2-9}$$

The X-data must have at least as many samples as variables, which becomes a problem in, e.g., spectroscopy due to the large number of wavelengths. Either a subset of variables has

to be used in the model (windowing) or the data should be condensed to a lower number of variables. The methods described in the following sections basically present a way to compress the data onto a fewer number of variables to be able to apply ILS to data sets with a large number of variables.

The calibration matrix $\hat{\mathbf{B}}$ can be used to find unknown concentrations of all analytes:

$$\hat{\mathbf{Y}}_{unk} = \hat{\mathbf{B}}\mathbf{X}_{meas} \tag{2-10}$$

Unlike CLS, ILS does not require concentration values for all analytes in the system. ILS does not account for all variation in the X-data but only for the variations caused by changes in the Y-variables of interest, implicitly accounting for variations in X-data originating from other sources. It has the ability to 'neglect' irrelevant variations in the data set to some extent, increasing its robustness over CLS models.

Principal component regression

To overcome the limitation of ILS for data sets with a large number of X-variables, the data set has to be compressed to a smaller number of X-variables. One way to do so is by combining PCA with ILS. This method is called Principal Component Regression (PCR). PCA is used to compress the data set and ILS is subsequently used for the regression step. In ILS, data compression can only be achieved using windowing. Data compression in PCR is accomplished by calculation of a reduced number of factors (or Principal Components (PCs)) from linear combinations of the original variables. The new factors are defined in such a way that the first factor has the largest possible amount of variance captured from the original data set and each succeeding factor covers the highest possible variance that is orthogonal to the preceding factor(s). This orthogonality eliminates the stability problems for collinear data sets that are experienced with the previously described methods.

The compression step is mathematically represented in equation (2-11), where $\mathbf{P}$ is the loadings matrix and $\mathbf{T}$ is the scores matrix, containing respectively the newly defined PCs in terms of the original variables and the intensities of each sample with respect to that PCs.

$$\mathbf{X} = \mathbf{T}\mathbf{P}^t + \mathbf{E} \tag{2-11}$$

The PCs are chosen in such a way that each sequential PC describes as much of the remaining variance in the X-data as possible. Data compression occurs when the number of used principal components is less than the number of original variables. Determination of the amount of principal components to be used is an optimization between a good explanation of the original data on the one hand and over-fitting of that data on the other.

The PCR model is calibrated using Equations 2-12 and 2-13 and the obtained regression matrix $\hat{\mathbf{B}}$ is then used to predict the unknown Y-data, using Equation 2-10.

$$\mathbf{Q} = (\mathbf{T}^t\mathbf{T})^{-1}\mathbf{T}^t\mathbf{Y} \tag{2-12}$$

$$\hat{\mathbf{B}} = \mathbf{P}\mathbf{Q} \tag{2-13}$$

The two main advantages of PCR over CLS and ILS are therefore that the stability problems with collinear data sets are eliminated and that the method can be applied for data sets with a large number of X-variables.

Partial Least Squares Regression

Partial Least Squares Regression (PLSR) is a widely applied regression tool in chemometrics. It is very much comparable to PCR with this difference that the factors are defined not only based on a maximum of variance in the X-data, but in both the X- and the Y-data. This is accomplished by maximizing the covariance between X and Y. The regression matrix then becomes:

$$\hat{\mathbf{B}} = \mathbf{W}(\mathbf{P}^t\mathbf{W})^{-1}\mathbf{Q} \tag{2-14}$$

The new matrix $\mathbf{W}$ contains the loading weights that are introduced to maintain orthogonal scores. The unknown Y-data can again be estimated using Equation 2-10. The newly constructed components in PLSR are called Latent Variables (LVs) and are equivalent to the principal components in PCR.

A distinct advantage of PLSR over PCR is that most often, simpler models (i.e. consisting of less components) can be built, that are as effective as more complex PCR models built from the same calibration data. PLS models are therefore generally more stable than PCR models. The need to use both the X- and Y-data in the definition of the LVs results, however, in increased complexity of the PLSR model calibration and expression. The PLSR-algorithms (for details refer to [28][29]) are therefore more complex than the simple two-step PCR algorithm. Another disadvantage of PLSR over PCR is the larger potential for over-fitting, especially if the Y-data is rather noisy. Critical in using PLS is the determination of the number of latent variables to be used.

2-3-3 Statistical diagnostics

Root-mean-square error

To assess and compare the quality of different chemometric models, and to decide on the number of components to be used, several performance indicators are proposed in literature. Most often, the Root-Mean-Square Error of Calibration (RMSEC) and the Root-Mean-Square Error of Prediction (RMSEP) are used for internal and external validation, respectively. The RMSE is defined as the square root of Predicted Residual-Sum-of-Squares (PRESS) divided by the number of degrees of freedom in the calibration.

$$RMSEC = \sqrt{\frac{\sum_{i=1}^{n}(\hat{y}_{i,cal} - y_{i,cal})^2}{d}} \tag{2-15}$$

$$RMSEP = \sqrt{\frac{\sum_{i=1}^{n} (\hat{y}_{i,val} - y_{i,val})^2}{d}} \tag{2-16}$$

In deciding on predictive model performance and number of components to be used in the developed models the RMSEP is used. The RMSEP is an indicator for the mean error in the predicted variables, expressed in the units of that variable.

Residuals and hotelling

Hotelling's T-Squared and Q-residuals are indicators that help to explain how well the model describes individual samples. Given a model as described in Equation 2-11, for a given observation i, the Q-residual is defined as

$$Q_i = \mathbf{e}_i \mathbf{e}_i^T = \mathbf{x}_i \left(\mathbf{I} - \mathbf{P}_k \mathbf{P}_k^T \right) \mathbf{x}_i^T \tag{2-17}$$

Where $\mathbf{e}_i^T$ is the ith row of the residual matrix $\mathbf{E}$ (see Equation 2-18) and $\mathbf{x}_i^T$ is the ith row of the data matrix $\mathbf{X}$.

$$\mathbf{E} = \mathbf{X} - \mathbf{T}\mathbf{P}^T \tag{2-18}$$

The Q-residual indicates how well each observation is matched by the model. It is therefore a lack-of-fit statistic, which can be used for outlier detection outside the calibration set. A high Q-value for a validation sample indicates that the respective sample might be an outlier.

The hotelling's T^2 values represent the variation of different observations within the model and can therefore be used to detect outliers within the calibration data set. For a model as described in Equation 2-11 it is defined as:

$$T_i^2 = \mathbf{t}_i \boldsymbol{\lambda} \mathbf{t}_i^T = \mathbf{x}_i \mathbf{P}_k \boldsymbol{\lambda}^{-1} \mathbf{P}_K^T \mathbf{x}_i^T \tag{2-19}$$

Where $\mathbf{t}_i$ is the ith row of the scores matrix $\mathbf{T}$ and $\boldsymbol{\lambda}$ is a diagonal matrix containing the eigenvalues corresponding with the components in the model (principal components or latent variables). High T^2 values indicates possible outliers within the calibration sample set.

Chapter 3

Experimental

3-1 Miniplant

The first continuous validation of the developed model was performed at the the Karlsruhe Institute of Technology (KIT). The TNO-owned mini carbon capture plant was operated there (Figure 4-3). A PID of the miniplant is provided in Appendix A-2 and a process description of the miniplant can be found in Section 4-2.

3-2 Microplant

Part of the validation experiments were carried out at the TNO microplant set-up. This set-up is a small CO_2 capture plant, mainly used for degradation related experiments. The microplant is depicted in Figure 3-1 and a PID is provided in Appendix A-1.

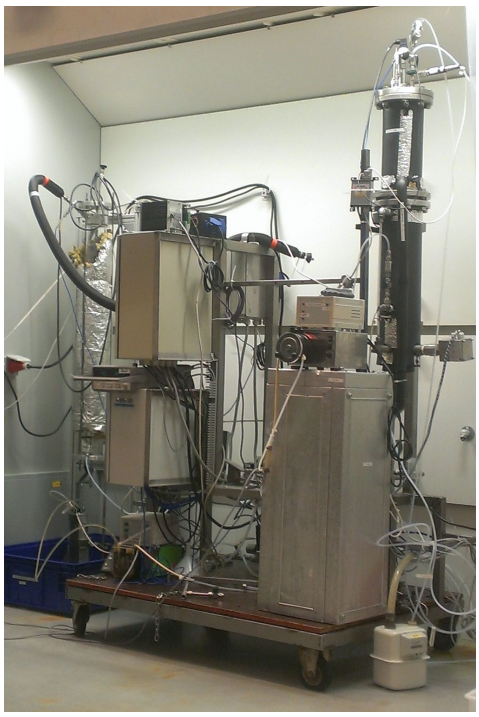

Figure 3-1: Picture of the microplant set-up

As indicated by its name, the microplant is a small scale CO_2 capture plant. The absorber and stripper have a height of approximately 1.2 [m] and an inner diameter of approximately 0.09 [m]. The total liquid volume in the system is around 8 [l], if the measurement loop is connected. Typical solvent flow rates in the microplant are around 6 [l/h], with an artificial flue gas flow of approximately 450 [l/h] consisting of 12 [vol%] CO_2 and 88 [vol%] air. The rich solvent, coming from the absorber, enters the absorber sump that contains around 1 [l] of solvent. The solvent is usually pumped from the absorber sump by the rich solvent pump (P202 in the PID diagram) and the liquid level in the sump is controlled by pump P201. This pump starts if a certain liquid level is reached. The rich solvent pump did not work during the experiments and therefore the entire flow was pumped by P201.

During the experiments, the test loop containing all measurement devices was switched between the lean and the rich flow. In the rich circuit, it was connected directly after the absorber sump, whereas in the lean, it was located after the lean-rich heat exchanger. The absorber was operated at atmospheric pressure and the stripper at 1.9 [bara] and 117 [°C]. The solvent temperature in the absorber depended on the amount of CO_2 captured by the solvent and was around 35-40 [°C].

3-3 Analytical techniques

Different analytical techniques were used in obtaining calibration and validation data for the developed models. All used analytical techniques are shortly described in this section, including the methods to analyze the MEA and CO_2 concentration in the different samples.

3-3-1 Density

The density of a substance is defined as its mass per unit volume:

$$\rho = \frac{m}{V} \tag{3-1}$$

For the offline density measurements a DMA 4500 Anton Paar oscillating tube density meter, with an accuracy of ±0.00005 [g/cm3] was used. This density meter uses the oscillating U-tube principle. The density is determined by measurement of the oscillation frequency of the tube containing a sample. The eigenfrequency of the oscillating tube is influenced by its mass and that principle is used to calculate the density of the inserted medium.

Inline density measurements were performed using CMF010 Elite MicroMotion coriolis flow and density meter. The accuracy of this device was ±0.0005 [g/cm^3] The density is measured in the same way as in the offline density meter. The natural frequency of the tubes in the coriolis meter changes with changes in the density of the flowing medium which can be deduced from that frequency.

3-3-2 Viscosity

Viscosity is a measure of the resistance of a fluid against deformation by shear or tensile stress. Hence the viscosity is the resistance of a fluid against a change of form, as can be seen from Equation 3-2. Viscosity is expressed in terms of dynamic (μ) or kinematic viscosity (ν).

$$\tau = \mu \left(\frac{\partial u}{\partial y} \right) \tag{3-2}$$

$$\nu = \frac{\mu}{\rho} \tag{3-3}$$

Measurements of the viscosity were conducted by means of a Low Shear 40 rheometer from Contraves, having an accuracy of ±1 [%] of the measured value. This rheometer uses the Couette principle. The medium is contained in a small cup in which a rotating cylinder is immersed. The resistive force that the medium exerts at the rotating cylinder is measured and used to calculate the viscosity of the medium. The cup is temperature controlled.

3-3-3 Conductivity

Conductivity, or electrical conductivity, is the opposite of electrical resistivity. It is a measure of the ability of a material to conduct an electric current and is expressed in terms of Siemens per length unit. The conductivity is generally defined as the magnitude of the current density divided by the magnitude of the electric field in a substance:

$$\sigma = \frac{J}{E} \tag{3-4}$$

A portable Orion Star A322 conductivity meter from ThermoScientific was used for offline conductivity measurements (±0.5 [%] of value). The online measurements were done using a SZ3274.168 EC probe combined with a C7635 conductivity controller having an accuracy of ±0.1 [mS/cm], both purchased from Nieuwkoop bv.

3-3-4 pH

The acidity of a substance is usually expressed in terms of pH. Solutions with a pH below 7 are said to be acidic and solution with a pH higher than 7 are said to be basic. Pure water has a pH of 7. The pH is defined as the negative logarithm of the hydrogen ion activity in a solution:

$$pH = -\log_{10}(a_{H^+}) = \log_{10}\left(\frac{1}{a_{H^+}}\right) \tag{3-5}$$

Offline pH measurements were carried out using a PHM210 from Radiometer Analytical. For online measurements a pH3630 transmitter was combined with a SZ165 pH probe, both from Nieuwkoop bv. Both analytical techniques have an accuracy of ±0.01 pH.

3-3-5 Refractive index

The refractive index is a number that describes the propagation of light through a medium. It is defined as the speed of light in vacuum divided by the speed of light in the medium (Equation 3-6). The refractive index is often reported as n_D20, were n stands for the refractive index, D for the wavelength of the used light (in this case the D line of natrium, or 589 [nm]) and 20 for the reference temperature in degrees centigrade. An inline brix refractometer (CM780N) from Atago was used for the brix measurements, which were subsequently converted to n_D20 values using an empirical correlation that was provided by Atago (Equation 3-7).

$$n = \frac{c}{v} \tag{3-6}$$

$$n_D 20 = 1.333 + 1.335 \times 10^{-3}(BRIX) + 7.608 \times 10^{-6}(BRIX)^2 \tag{3-7}$$

The accuracy of the used analytical device was ±0.1 [%].

3-3-6 Speed of sound

The speed at which sound waves propagate through a medium is called the speed of sound in that medium. It is thermodynamically defined as the partial derivative of pressure with respect to density, taken adiabatically:

$$c^2 = \left(\frac{\partial p}{\partial \rho}\right)_s \tag{3-8}$$

Speed of sound measurements were done using three different analytical devices. Two Olympus 5 [MHz] transducers combined with a LeCroy 9400A scope and an ultrasonic analyzer were used to conduct the sonic speed measurements in the screening experiments. The transducers were placed at in a water bath at a distance of 0.2 [m] from each other and the sample was placed in between. The sample was contained in a PVC cup with a width of 0.015 [m], covered with thin adhesive plastic. This thin plastic was used because it has negligible influence on the obtained measurement results. Sonic speed data was obtained by comparing the time between the sending and receiving of a sonic signal with and without the sample. Due to apparatus limitations, this technique could only be applied at room temperature.

For the calibration experiments a LiquiSonic lab system from SensoTech was used. The inline measurements of the speed of sound were conducted using a SensoTech LiquiSonic 20 controller, combined with an immersion type probe 40-40. Both probes measure the sonic speed by measurement of the time between sending and receiving a sonic signal over a fixed distance. The measurement accuracy for both probes was ±0.1 [m/s]. The probe that was used inline was contained in a specially fabricated metal cup. The cup had an inner diameter of 0.08 [m] and a liquid level height of around 0.10 [m].

3-3-7 NIR spectroscopy

near infrared (NIR) spectroscopy uses the near-infrared region of the electromagnetic spectrum (typically 800 to 2500 [nm]). It is typically applied in pharmaceutical and medical applications as well as in quality control of e.g. food. A NIR256-2.0 AvaSpec spectrometer from Avantes was used to obtain the NIR spectra, with an AvaLight-HAL tungsten light source and a dip probe and flow cell, for offline and online measurements respectively (light source accuracy ±0.1 [%], photometric accuracy ±1 [%]). The bandwidth of this spectrometer was 1016 to 2045 [nm]. Averaging was done over 10 spectra and the integration time was 20 [ms]. The collected spectra were converted to absorbance spectra using Equation 3-9.

$$A_n = -\log\left(\frac{sample_n - dark_n}{ref_n - dark_n}\right) \tag{3-9}$$

The dark spectrum was collected with the light source switched off and water was used for the reference spectrum.

3-3-8 UV-vis spectroscopy

The part of the electromagnetic spectrum located at the boundary of the visible and the ultraviolet is used in UV-vis spectroscopy. Most liquid- and gas-phase UV-vis spectroscopic measurements rely on Beer's Law, in which the light absorbance is expressed in terms of the molar absorption coefficient, the pathlength and the concentration of different species in the medium.

$$A = \epsilon b C \tag{3-10}$$

An Ultrospec 2100 pro from GE Healthcare was used to collect the UV-vis spectra, with a bandwith of 201 to 900 [nm]. The wavelength accuracy was ±1 [nm] and the photometric accuracy ±0.5 [%]. This apparatus is only able to perform spectroscopy on lab samples and not for online purposes.

3-3-9 Analysis of MEA concentration

The MEA concentration is determined using a Titralab TIM965 titration manager, with an accuracy of ±0.7 [%], combined with a SAC850 sample changer, both from Radiometer Analytical. A solution of 0.1 [M] HCl is used as titrant. 100 [μl] of a sample is diluted with 25 [ml] water and 1 [ml/min] of titrant is added until the deflection point has been reached. Given the amount of titrant added to reach the deflection point, the molarity of MEA in the sample is found and the mass concentration can be calculated if the density of the sample is known. The MEA concentration with respect to the unloaded solution is subsequently found using the CO_2 concentration. The combined accuracy of this method (amount of sample added included) was considered to be ±2.5 [%]

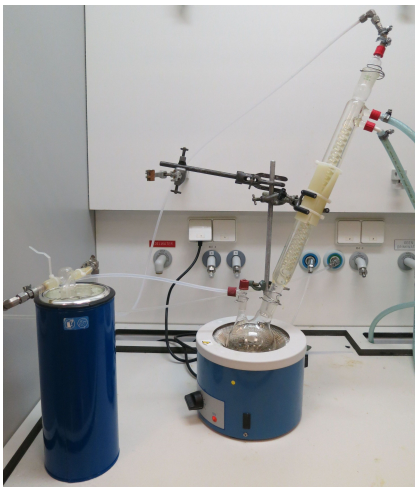

Figure 3-2: The phosphoric acid set-up for CO_2 concentration analysis

3-3-10 Analysis of carbon dioxide concentration

To determine the CO_2 concentration in a sample the phosphoric acid set-up is used (Figure 3-2). 5 [ml] of a sample is injected in the flask, containing boiling phosphoric acid. A nitrogen flow of 400 [l/h] is circulated through the flask. All CO_2 is released from the sample when it contacts the phosphoric acid and it is subsequently transported to a Rosemount BINOS 100 2M CO_2 analyser with the nitrogen flow. The amount of released CO_2 is analyzed and used to calculate the molar concentration of CO_2 in the sample. With a known density, the mass concentration of CO_2 in the sample is obtained. The accuracy of this method was rather low due to many disturbing influences and was considered to be ±5 [%].

Chapter 4

Model development and validation

4-1 Introduction

This chapter deals with the development and validation of the predictive chemometric model to determine the Monoethanolamine (MEA) and CO_2 concentrations in the solvent in real-time. The model development and validation was divided into five parts:

1. Sensitivity assessment
   Investigation of different analytical techniques to be used in model development
2. Construction of a calibration data set
   Preparation of calibration samples and measuring of required solvent properties
3. Calibration and development of the final model
   Utilization of the calibration data set to calibrate and develop a chemometric model
4. Validation of the developed model by means of lab-samples
   Offline validation of the predictive accuracy of the developed model
5. Online validation of the developed model at the miniplant
   Experiments at a CO_2 absorbing miniplant, operated at the the Karlsruhe Institute of Technology (KIT)

The process and results of model development and validation have been described in a manuscript that was submitted to Industrial & Engineering Chemistry Research (IECR). The submitted manuscript is presented in section 4-2, the appendices are to be found in Chapter B.

4-2 Submitted manuscript

Online Monitoring of Solvent and Acid Gas Concentration in a Carbon Dioxide Absorption Process using Monoethanolamine

Andries C. van Eckeveld[†,§], Leen V. van der Ham[†], Leon F.G. Geers[‡], Leo J.P. van den Broeke[ϟ] , Bendiks J. Boersma[§], Earl L.V. Goetheer[†]

†TNO Gas Treatment, Leeghwaterstraat 46, 2628CA Delft, The Netherlands
‡TNO Process and Instrumentation Development, Leeghwaterstraat 46, 2628CA Delft, The Netherlands
ϟQatar University, Department of Chemical Engineering, Jamaa Street 2713, Doha, Qatar
§Delft University of Technology, Process and Energy Department, Leeghwaterstraat 44, 2628AC Delft, The Netherlands

Abstract

A method has been developed for online liquid analysis of the amine and absorbed CO_2 concentrations in a post-combustion capture process using monoethanolamine as a solvent. Online monitoring of the dynamic behaviour of these parameters is of major importance in process control and is currently only achieved using expensive Fourier transform infrared spectroscopy. The developed method is based on cheap and easy measurable quantities. Inverse least-squares models were built at two temperature levels, based on a set of 29 calibration samples with different MEA and CO_2 concentrations. Density, conductivity, refractive index and sonic speed measurements were used as input data. The developed model has been validated during continuous operation of a mini CO_2-capture pilot-plant. Concentrations of MEA and CO_2 were predicted with an accuracy of 0.53 [wt%] and 0.31 [wt%], respectively. Process dynamics, like step-changes in the CO_2 flue gas concentration, were covered accurately as well. The model showed good robustness to changes in temperature. Combining density, conductivity, refractive index and sonic speed measurements with a multivariate chemometric method enables the real-time and accurate monitoring of the acid gas and monoethanolamine concentrations in CO_2 absorption processes.

1 Introduction

Capturing CO_2 from industrial flue gases has a great potential in reducing the emission of this major greenhouse gas into the atmosphere[5]. One of the ways to capture CO_2 is Post-Combustion Capture (PCC) using an amine based-chemical absorption process[30]. In such a process, the CO_2 in the flue gas reacts with the aqueous amine solution, which is regenerated again at elevated temperature and pressure. The process generally consists of an absorber and a stripper column, as depicted in Figure 4-1. The flue gasses are brought in contact with the solvent in the absorption column (C1), where the CO_2 reacts with the solvent. The cleaned flue gas is purged and the CO_2-rich solvent is heated in the lean-rich heat exchanger (H1) and subsequently regenerated in the stripper column (C2). The CO_2 is thermally stripped from the solvent and the lean solvent is cooled in the lean-rich heat exchanger and recycled to the absorber. In this work, chemical absorption with an aqueous MEA solution as absorbing agent is used as a base case.

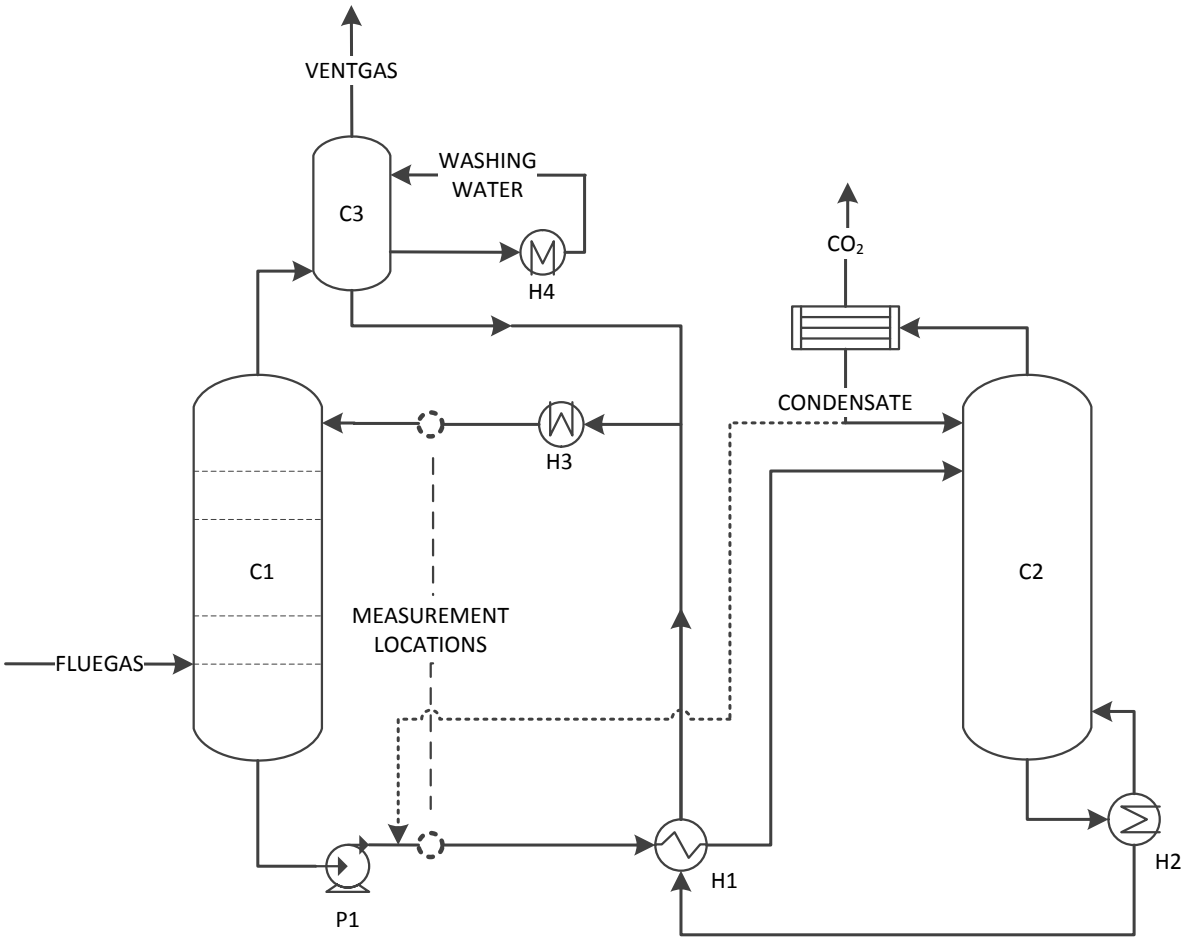

Figure 4-1: Flow sheet of a typical amine-based CO_2 capture process. Dotted condensate return line represents the installation in the TNO mini-plant

Although this PCC process is in principle not very complicated, controlling its performance is not an easy task. First, the flue gas composition and flow rate fluctuate due to upstream operational variations in the (power) plant. Second, solvent degradation and deactivation occurs, induced by elevated temperatures in the process and by irreversible reactions with other species present in the flue gas (e.g. O_2, SO_x and NO_x) or CO_2 [31, 32], leading to a reduction in capture capacity. Controlling process performance, therefore, requires accurate monitoring of the absorbent and CO_2 concentrations in the liquid phase. Current methods (based on offline lab analysis) are laborious and fail to cover fast transient behavior in the solvent composition. fourier transform infrared (FTIR) combined with a multivariate chemometric method to predict these concentrations online for PCC processes exploiting the potassium salt of β-Alanine[8] and MEA[9] as absorbents. The obtained results were promising with respect to the predictive accuracy. However, there are some disadvantages related to the use of FTIR: first, the relatively high costs of the required apparatus and second, the need for it to be located within a few meters of the process. Furthermore, the method shows unsatisfactory results when the concentrations of the components in the mixture exceed respective calibration limits, or when the mixture contains components the model was not calibrated for.

A more cost-effective method for determination of solvent and solute composition in the liquid can be found in the combination of easy measurable solvent properties with a multivariate chemometric method. Previously, some work has been done using different analytical techniques to determine solvent composition. Conductivity measurements have been used for CO_2 concentration monitoring[10, 11], but the use of one analytical technique restricts the possible prediction to only one component. A combination of density and refractive index measurements has been evaluated for estimation of the solvent and solute concentrations in amine based CO_2 capture processes[12] and the results were promising in terms of predictive accuracy. However, the robustness of this technique to disturbances is limited due to the inclusion of only two measured quantities. The sensitivity of sonic speed to amine concentration was identified by Hawrylak et al.[13] and sonic speed might therefore be applicable for the prediction of the amine concentration in the solvent. Recently, a screening study has been carried out to assess the sensitivities of different simple analytical techniques to compositional changes in the solvent mixture[14]. Assessed solvent properties were conductivity, pH, density, refractive index and UV-vis spectra. Combinations of density, refractive index, conductivity and pH showed promising results for predicting the MEA and CO_2 concentrations of solvent samples. No method has been reported concerning the online prediction of solvent composition, which is both cost effective and readily implemented. The objective of this work is to develop a real-time model that enables monitoring of the absorbent concentration and acid gas loading, based on solvent properties that are relatively inexpensive and easy to measure.

This paper is organized as follows. The method to come to a predictive model is described in Section 2. Used chemical and the experimental procedure is treated in Section 3, followed by the results and model calibration in Section 4. Finally, the model validation is described in Section 5 and the paper is concluded in Section 6.

2 Approach

To come to a predictive model for the MEA and CO_2 concentration in a carbon capture process, first screening experiments were carried out. The sensitivity of density, conductivity, pH, viscosity, sonic speed, refractive index, near infrared (NIR) spectroscopy and visible ultra-violet (UV-vis) spectroscopy to changing solvent composition and the presence of contamination was assessed. The MEA and CO_2 concentrations were the most important variables included in these screening experiments. In addition, five other factors were included to account for solvent degradation, deactivation and temperature. Nitric acid (HNO_3) and sulfuric acid (H_2SO_4) are the third and fourth factor. They are the main contaminants resulting from the presence of NO_x and SO_x in flue gasses and are also known to form Heat Stable Salts (HSS) with MEA. According to Rochelle et al.[17], 1-(2-hydroxyethyl)imidazolidone-2 (HEIA) is one of the major products from the thermal degradation pathway called carbamate polymerization and is, therefore, included as well. Next to that, a pollutant mix is added as the sixth factor, containing common oxidative degradation products: ammonia, formic acid, formaldehyde, acetic acid and oxalic acid[33]. Temperature is included as the seventh factor to evaluate the dependence of the analytical techniques on temperature changes.

Assessing the relations between seven parameters at two levels (low and high) would involve $2^7 = 128$ different samples. To reduce the number of required samples, the design of experiments approach is used[34]. A two-level (high and low), seven-factor fractional-factorial DOE was

developed, having a resolution of IV. This means that first order-interactions are confounded with third-order interactions and second-order interactions with each other. Only first order effects can be investigated following this approach. This is not problematic, since the first-order sensitivities were the main interest of these screening experiments.

Table 4-1: High and low values used in the design of the screening experiments. Concentrations are with respect to the total solution.

Factor	Low value	High value
MEA [wt%]	25	35
CO_2 [wt%]	0	5
HNO_3 [wt%]	0	1
H_2SO_4 [wt%]	0	1
HEIA [wt%]	0	1
Pollutants consisting of		
Ammonia [wt%]	0	0.25
Formaldehyde [wt%]	0	0.25
Formic acid [wt%]	0	0.50
Acetic acid [wt%]	0	0.50
Oxalic acid [wt%]	0	0.25
Temperature [°]	20	60

Sixteen samples are required following this approach, accompanied by a center point sample. The high and low levels for all seven factors are listed in Table 4-1, where the concentrations are in mass percentages of the total solution. The MEA concentration in actual absorption processes is usually around 30 [wt%] and the high and low concentrations are chosen around this value. The maximum CO_2 concentration depends on the MEA concentration and is chosen to be 5 [wt%] of the total solution. This concentration is for all samples smaller than the maximum concentration of 0.5 mole per mole MEA, which allows the free MEA to react with added contaminants. Desorption of CO_2 due to the addition of contaminants will, therefore, be negligible. The added amounts of pollutants, HNO_3, H_2SO_4 and HEIA are small and only aimed to assess the influence of these components on the measurement results. The chosen concentrations do not reflect actual concentrations occurring in process plant operation.

Sensitivities of all measurement techniques were assessed with respect to the MEA and CO_2 concentrations and their robustness against pollution and contamination. In order to do so, a sensitivity parameter was computed from the measurement data. The measurement results were first multiplied with a 1 or -1 for a high or low level in the DOE, respectively, and were subsequently summed for each factor separately. This resulted in a number that represents the change in a measured quantity due to an increase in the respective factor. Dividing this value by the standard deviation of the corresponding measured property resulted in a sensitivity parameter that allows for a comparison between all measured quantities. The obtained sensitivity parameter was used to investigate the applicability of the different analytical techniques in predictive modeling of the MEA and CO_2 concentration in the solvent.

For subsequent model calibration and validation 29 samples were prepared containing different MEA and CO_2 concentrations. No other components were added to the samples, because only the MEA and CO_2 concentration were to be quantified by the model. Seventeen of these samples were used in model calibration and the remaining were used for model validation. The applied ranges for MEA and CO_2 and the temperature used in model calibration are typical for chemical absorption plants exploiting MEA as absorbent. Most commonly, MEA concentrations of around 30 [wt%] are used in process plants. Higher concentrations are rarely applied and the MEA concentration range is therefore defined to be 20-36 [wt%] MEA as a function of the fresh and unloaded solution. It is common practice in this kind of processes to express the concentration of the absorbing agent in terms of the unloaded solution and this

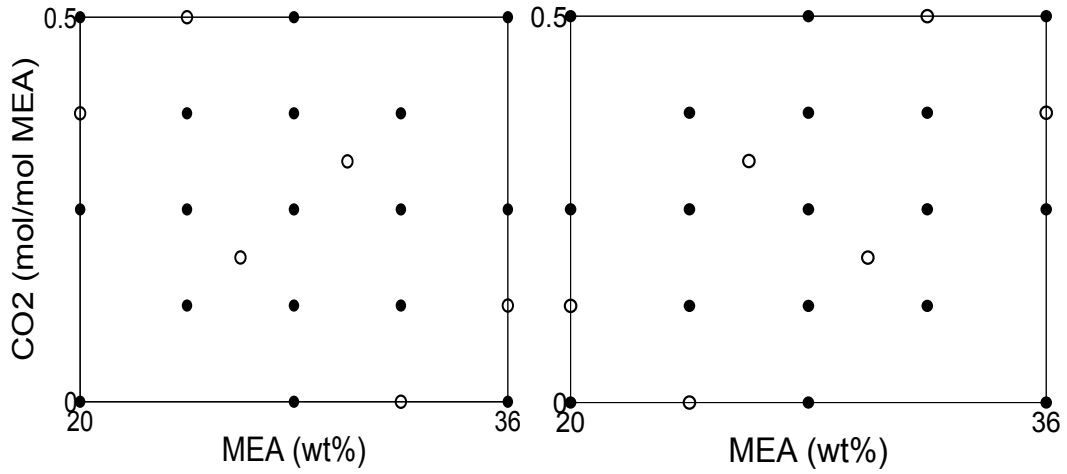

Figure 4-2: Model development sample distribution for 40 [°C] (left) and 55 [°C] (right). Filled dots represent calibration samples, open dots represent validation samples.

convention is followed here. CO_2 concentrations are defined as molar loading of MEA. The applied range is 0 - 0.5 mole per mole MEA. The sample set was divided into two sets of 23 samples, as indicated in Figure 4-2, one of these sets was used for model development at 40 [°C] and the other for model development at 55[°C]. The chosen temperatures are typical for, respectively, the lean and rich solvent flows at the measurement positions indicated in Figure 4-1.

Several chemometric models were created using the calibration data to evaluate the predictive performance of different combinations of analytical techniques. The best performing model is subsequently evaluated during two continuous trials on a mini capture plant and finally validated using manual offline analysis.

3 Materials and experimental procedure

3.1 Used Chemicals

MEA (99%), HEIA (75%), sulfuric acid (65%), ammonia (28-30%), formaldehyde (37%), acetic acid (99.5%) and oxalic acid (0.5 [M]) were purchased from Sigma-Aldrich. Formic acid (98-100%) was purchased from Merck and nitric acid (65%) from Fluka. All chemicals were used as received.

3.2 Sample analysis

The MEA concentration in the samples is measured using titration with HCl. A TIM965 titration manager from Radiometer Analytical is used for this purpose. CO_2 concentrations were obtained by injecting a known quantity of the sample into boiling phosphoric acid, releasing all the dissolved CO_2. The amount of CO_2 in the gas phase is continuously measured using a Binos 100 2M carbon dioxide analyzer from Rosemount Analytical. Accuracy of these analytical techniques is $\pm 2.5\%$ and $\pm 5\%$ of the measured values, respectively.

3.3 Screening experiments

The samples have been prepared in an ice-bath and under a nitrogen blanket, to prevent any unwanted side reactions to occur. A loaded and unloaded MEA stock solution was made, containing 50 [wt%] MEA and a CO_2 loading for the loaded solution of 0.5 mole per mole MEA. The main contaminants (HNO_3, H_2SO_4 and HEIA) were diluted to 25 [wt%] before being added to the samples. All mentioned concentrations are in [wt%] of the entire solution. The samples were prepared from these stock solutions and the pollutants mix, which was prepared by addition of individual pollutants to demineralized water. The samples were heated to the required temperature before measurements were conducted.

Densities were measured using a DMA 4500 Anton Paar oscillating U-tube density meter. Conductivity measurements were performed using the Orion Star A322 portable conductivity meter from Thermo Scientific, with a linear temperature correction of 2.1 [$^{\%}/_{\circ C}$]. pH was measured with a PHM210 pH meter from Radiometer Analytical. An inline brix refractometer (CM780N) produced by Atago was used for the brix measurements (BRIX), which were converted to refractive index (n_D20) values using the following empirical correlation, provided by Atago:

$$n_D20 = 1.333 + 1.335 \times 10^{-3} \times (BRIX) + 7.608 \times 10^{-6} \times (BRIX)^2 \tag{4-1}$$

Viscosities were measured using a Contraves Low Shear 40 viscometer. NIR spectra were obtained using an Avantes AvaSpec NIR256-2.0 spectrometer, operated with an AvaLight-HAL tungsten halogen light source and a dip probe. The wavenumber range of the resulting spectra was 4891-9833 [cm^-1]. Integration time was 20 [ms] and averaging was done over 10 spectra. UV spectra were measured using the Ultrospec 2100 pro from GE Healthcare, with wavelengths ranging from 210 to 900 [nm]. Two Olympus 5 [MHz] transducers combined with a LeCroy 9400A scope and an ultrasonic analyzer were used to conduct the sonic speed measurements. The transducers were placed in a water bath facing each other and the sample was placed in between. The sample was contained in a PVC cup, covered with thin adhesive plastic. This thin plastic has negligible influence on the obtained measurement results. Sonic speed data was obtained by comparing the time between sending and receiving a sonic signal with and without the sample. Due to apparatus limitations, the sonic speed was measured at room temperature only.

3.4 Calibration experiments

The samples used for model calibration were prepared from two stock solutions, containing 40 [wt%] MEA of the fresh (unloaded) solution. One of the stock solutions was loaded with 0.526 mole CO_2 per mole MEA (or 12.6 [wt%] CO_2 of the total solution). The samples were prepared from the stock solutions in air and at room temperature. The samples were subsequently heated to the respective temperature levels (40 [°C] or 55 [°C]). Required measurements were done and the acquired data was used for model calibration and assessment (Section 4.2).

The analytical techniques were the same as in the screening experiments except for sonic speed. A LiquiSonic Lab system from SensoTech was used to measure the sonic speed in the samples. This technique could also be used at elevated temperatures, required for the calibration measurements.

3.5 Continuous trial

Model validation is carried out at the TNO mini absorption plant[35]. A picture of the absorber and stripper column of that plant is given in Figure 4-3. The flow-sheet of this pilot plant is shown in Figure 4-1, where the dotted line represents the condensate return line in the mini-plant set-up. Artificial flue gas was fed to the absorber packed column, were CO_2 was absorbed in the aqueous MEA solution. The cleaned flue gases were vented into the atmosphere. The rich (loaded) solvent was heated and then fed to the desorber, where the dissolved CO_2 was released at elevated temperature and pressure. The lean solvent was subsequently recirculated to the absorber. Specifications of the plant are given in Table 4-2. The plant was operated with aqueous MEA as solvent and an artificial flue gas flow containing a mixture of CO_2 and air. The measurement loop consisted of density, pH, conductivity, NIR and refractive index sensors. During the first test run, it was installed in the lean stream, directly after the lean cooler (H3 in Figure 4-1). For the second test run it was moved to the rich stream, after the absorber bottom pump. Refractive index and NIR measurements were conducted using the same apparatus as for the calibration experiments.

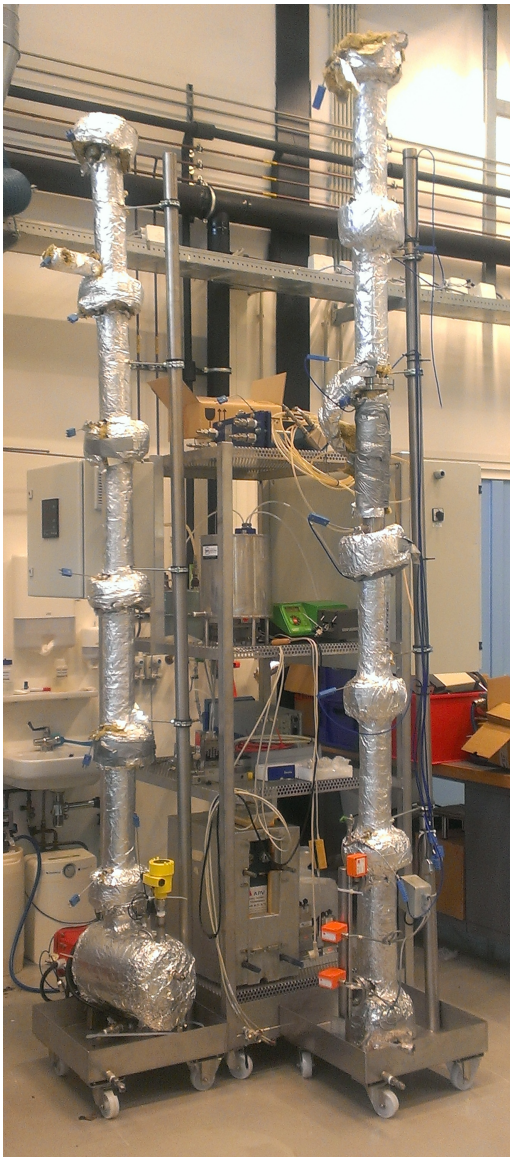

Figure 4-3: Miniplant absorber (left) and stripper column

Inline density measurements were done using an Elite MicroMotion Coriolis flow and density meter. Conductivities were measured using a SZ3274.168 EC probe combined with a C7635 microprocessor, both from Nieuwkoop bv. pH was measured using a SZ165 probe and a PH3630 transmitter, also from Nieuwkoop bv. Due to an incompatibility with the measurement apparatus, the sonic speed measurements were not performed inline; they were done on manually taken samples. These samples were also used to validate the models by analyzing the MEA and CO_2 concentrations as described in Section 5. During the measurements, twelve samples were taken; three during the first run and nine during the second run.

4 Results

4.1 Screening experiments

The obtained sensitivity results are listed in Table 4-3, and the quantities that are most sensitive to changes in different parameters can be identified. The sensitivity parameter has a value between -1 and 1, which indicates the sensitivity of a specific measured property for changes in the respective parameter. A sensitivity close to -1 or 1 indicates that the relation between a measured property and a changed parameter is very strong. For the UVvis and NIR, the sensitivity was calculated for the entire spectra, but the results for only two wavelengths (from the entire spectra) are listed in Table 4-3, having the largest sensitivities with respect to the MEA and/or CO_2 concentrations.

Table 4-2: Specifications mini-plant

Absorber height [m]	3.5
Absorber inner diam. [m]	0.045
Stripper height [m]	3.0
Stripper inner diam. [m]	0.045
Liquid circulation rate [kg/h]	15
liquid volume [l]	20

Table 4-3: Sensitivity results from screening experiments

Property	MEA	CO_2	HNO_3	H_2SO_4	HEIA	Pollutants	Temperature
Conductivity	-0.31	0.78	0.23	0.18	-0.03	0.29	0.16
pH	0.09	-0.54	-0.14	-0.15	-0.04	-0.22	-0.69
Density	0.06	0.88	0.10	0.15	0.04	0.14	-0.32
Refractive index	0.63	0.69	0.09	0.08	0.05	0.19	0.07
Viscosity	0.44	0.33	0.07	0.06	-0.02	0.04	-0.71
Sonic velocity	0.74	0.54	-0.03	0.06	0.12	0.19	-
NIR 5975 [cm^{-1}]	0.32	0.74	0.01	0.04	-0.07	0.16	-0.50
NIR 6922 [cm^{-1}]	-0.92	-0.19	-0.05	-0.04	-0.04	-0.18	0.05
UV-vis 270 [nm]	0.11	0.63	0.49	-0.14	0.06	0.28	0.29
UV-vis 300 [nm]	0.07	0.17	0.93	0.06	0.01	0.09	0.11

Temperature has a large effect on certain measured quantities. However, since the temperature is normally already measured inline in process plants it can be accounted for by the developed model and will, therefore, not be discussed in more detail.

From Table 4-3 it follows that conductivity measurements showed a large sensitivity to the CO_2 concentration in the solvent. Furthermore, it was sensitive to pollutants and contaminants in the samples and might therefore be used to identify solvent degradation and to limit its impact on model accuracy. The pH showed also a large (but negative) sensitivity to the CO_2 concentration and a somewhat lower sensitivity to contaminants in the solvent. The sensitivity for MEA was quite low for especially pH and density measurements, the latter of which, however, was very sensitive to changes in the CO_2 concentration. Refractive index was both sensitive to MEA and CO_2 concentrations and relatively robust to pollution, making it an attractive option in model development. The small sensitivity of viscosity measurements to contamination of the samples was encouraging, but due to a lack of availability of inline viscometers it is not used in further model development. Measurements of the sonic speed were sensitive to MEA concentration and a combination of sonic speed with density measurements is a promising option in estimating both MEA and CO_2 concentrations.

The UV-vis spectra showed a large sensitivity for mainly HNO_3 and CO_2 in certain wavelength ranges, but when it comes to MEA this sensitivity was limited. Furthermore, degradation causes the sample color to darken, indicating that a large amount of the visible light is absorbed in the samples. UVvis spectroscopy is therefore not adequate in process plant operation, where degradation occurs. NIR spectroscopy appeared to be sensitive to both MEA and CO_2 concentrations for certain wavelength ranges and pollutants and contaminants had a small influence on the obtained measurement results, for most wavelengths.

The described results are comparable with the sensitivities obtained by van der Ham et al.[14]. Differences occur for mainly conductivity and pH measurements. As mentioned in Section 3.3, a linear temperature correction was used for the conductivity measurements, which caused the, in this work obtained, sensitivity results of the conductivity to differ from the sensitivity obtained by van der Ham et al. The pH measurements were found to be less sensitive to both MEA and CO_2 concentration and more sensitive to temperature. Differences in experimental procedure might be causing these deviations. In addition to the previous work done by van der Ham et al., sonic speed, viscosity and NIR spectra were added to the screening experiments in this work. The presence of the carbamate polymerization product HEIA, which was not included in previous work, appeared to have a small influence on the assessed quantities compared to the other contaminants and pollutants, as follows from Table 4-3.

Based on the results of the screening experiments, only UV-vis and viscosity were excluded from further model development. Included were density, conductivity, pH, refractive index, sonic speed and NIR measurements.

4.2 Model calibration

The acquired calibration data is used to construct chemometric models based on different combinations of solvent properties, in order to assess which combination can best be used to calibrate the model, in terms of costs and predictive accuracy.

The performance of the developed models was compared based on the Root-Mean-Square Error of Prediction (RMSEP), for the validation samples:

$$RMSEP = \sqrt{\frac{\sum_{i=1}^{n} (\hat{y}_{i,val} - y_{i,val})^2}{n}} \tag{4-2}$$

Where n is the number of samples, Y_i is the measured and $\hat{y}_i$ the predicted value for the respective variable. The RMSEP represents the mean predictive error in the units of the respective predicted (or Y)-variable, in this case in weight percentage of the fresh solvent for MEA and in weight percentage of the total solution for CO_2.

All initially developed models were based on Partial Least Squares Regression (PLSR)[36]. This technique makes use of the inverse calibration approach, where it is possible to calibrate for the desired components while implicitly accounting for the other sources of variation. The data compression step in PLSR is bilinear, meaning that both the X- and Y-block data (or observed and predicted data) are projected onto newly defined Latent Variables (LVs). The latent variables are constructed based on maximum of variance captured in both the X- and Y-block data. The optimal number of latent variables to be used is determined iteratively using

the RMSEP for the validation samples as judging parameter. Since PLSR is an essentially linear technique, it is only able to model linear or weakly non-linear relations. Most measured quantities, however, have a non-linear temperature dependency resulting in reduced accuracy for non-calibrated temperature levels. It was therefore decided not to include temperature as a variable in the X-data but to develop models at two constant temperature levels (40[°C] and 55[°C]). For optimal model performance the measurement loop temperature should, therefore, be maintained at one of the calibrated values.

Data pre-treatment was different for NIR spectra and the other measurement data. The raw NIR data was first converted to absorbance spectra using

$$A_n = -\log\left(\frac{sample_n - dark_n}{ref_n - dark_n}\right) \tag{4-3}$$

where A_n is the absorbance spectrum of sample n, $sample_n$ is the raw NIR spectrum of the sample and ref_n and $dark_n$ are a reference and dark spectrum. Demineralized water was used as a reference. The absorbance spectra were subsequently windowed to exclude wavelength ranges where MEA and CO_2 concentration differences had no influence on the amount of absorbed light. The resulting spectra in the wavenumber range of 5271 - 8313 [cm^{-1}] were block scaled instead of variance scaled to preserve the mutual inner dependencies. Different filtering techniques were assessed. The use of first or second order derivatives of the spectral data is a common way to remove, respectively, baseline offset and global trend from the spectral data. Other proposed NIR spectral filtering techniques include Multiplicative Scatter Correction (MSC), Standard Normal Variate (SNV)[37] and Orthogonal Signal Correction (OSC)[38]. MSC and SNV are correction techniques for light reflections and scattering that affect the NIR spectra. Spectral variations that are unrelated to the concentrations of the species of interest are removed using OSC filtering. All mentioned preprocessing techniques were assessed for their influence on the RMSEP of the resulting model.

The other measurement data was z-scored by mean-centering and variance scaling. Mean centering was applied to remove unwanted leverage effects from the data and to focus on the differences in data induced by changes in Y-variables. Subsequent variance scaling removed weighing that was artificially induced by the scales of the measured quantities.

The obtained RMSEP for a selection of the assessed data sets is listed in Table 4-4. For the NIR data, only the models based on the first and second-order derivative of NIR and the unfiltered NIR data are reported in the table. The other filtering techniques showed comparable or worse predictive accuracy. The RMSEP values obtained by Geers et al. 5 , using the FTIR data, are reported in the last row of Table 4-4. These values were scaled to the absorbent and acid gas ranges used in this study, for comparability purposes.

From Table 4-4 it follows that the best-performing model at 40 [°C], in terms of RMSEP, was the model based on a combination of all assessed quantities, but exclusion of the NIR data gave only a slight increase in RMSEP. Models based on solely NIR data performed worse than most models based on the other data. The smallest predictive error based on the non-spectroscopic measurements was obtained using only density, pH, refractive index and sonic speed data for model calibration. At 55 [°C], the model based on density, conductivity, refractive index and sonic speed showed a comparable performance with the model based on all data. Other combinations of measurement data had a considerably higher RMSEP for

Table 4-4: RMSEP values for the developed models for 40 [°C] (left) and 55 [°C] (right)

Included data	RMSEP MEA [wt%]	RMSEP CO_2 [wt%]
All	0.13/0.42	0.03/0.11
NIR	0.22/0.63	0.11/0.08
1^{st} derivative of NIR	0.27/0.52	0.08/0.11
2^{nd} derivative of NIR	0.27/0.47	0.09/0.12
Density/pH/cond./refr. ind./sonic speed	0.17/0.53	0.04/0.12
Density/cond./refr. ind./sonic speed	0.24/0.44	0.05/0.11
Density/refr. ind./sonic speed	0.19/0.89	0.05/0.12
Density/pH/refr. ind./sonic speed	0.15/0.86	0.04/0.12
FTIR *(obtained by Geers et al.)*[8]	0.38	0.26

especially MEA. Remarkable is the large difference in accuracy between the models at 40 [°C] and 55 [°C]. Calibration measurements were carried out in air, possibly resulting in the absorption of uncalibrated species from air (oxygen/nitrogen) that could disturb the models. Higher temperatures influence the equilibrium concentration of these species and, possibly, enforce reactions in the samples. The effect of these temperature related changes depends on the time the sample has been heated which was not constant over all samples, thereby inducing uncertainties to the calibration data. Consequently, the models calibrated at 55 [°C] were less accurate, but more robust to disturbances. The final model was, therefore, calibrated using measurements of the density, conductivity, refractive index and sonic speed. These four techniques were chosen for model robustness purposes and to reduce apparatus costs. Estimated costs for the different measurement techniques are summarized in Table 4-5 and it follows that exclusion of NIR is advantageous in terms of costs, since the NIR spectrometer is the most expensive analytical technique used. The accumulated costs of the four analytical techniques is estimated to be around €16,000, representing a more than six times reduction compared to the use of FTIR alone.

Table 4-5: Estimated purchase costs of analytical equipment

Conductivity [€]	650
pH [€]	550
Density [€]	3,500
Refractive index [€]	5,000
Sonic speed [€]	7,000
NIR [€]	20,000
FTIR [€]	100,000

All models calibrated at 40 [°C] showed significantly increased predictive accuracy compared to that obtained by Geers et al. The 55 [°C] models were slightly less accurate in MEA but more accurate in CO_2 concentration prediction. The obtained predictive accuracy in this work is promising when it comes to process control purposes.

Figure 4-4 shows the predicted versus measured concentrations for both MEA and CO2 in the 40 [°C] and 55 [°C] cases. The confidence intervals for the predicted concentrations were constructed following the hetroscedastic error of prediction theory presented by Faber et al[39].

Since the model based on density, conductivity, refractive index and sonic speed consisted of four latent variables based on four X-variables, no data compression was required. Therefore an Inversed Least Squares (ILS) model was built instead of a PLSR model. The regression step in such a model is the same as for PLSR, but no data compression step is involved.

The final model is an ILS model, calibrated with density, conductivity, refractive index and

sonic speed measurement data of 29 calibration samples. The model was calibrated at two temperature levels: 40 [°C] and 55 [°C].

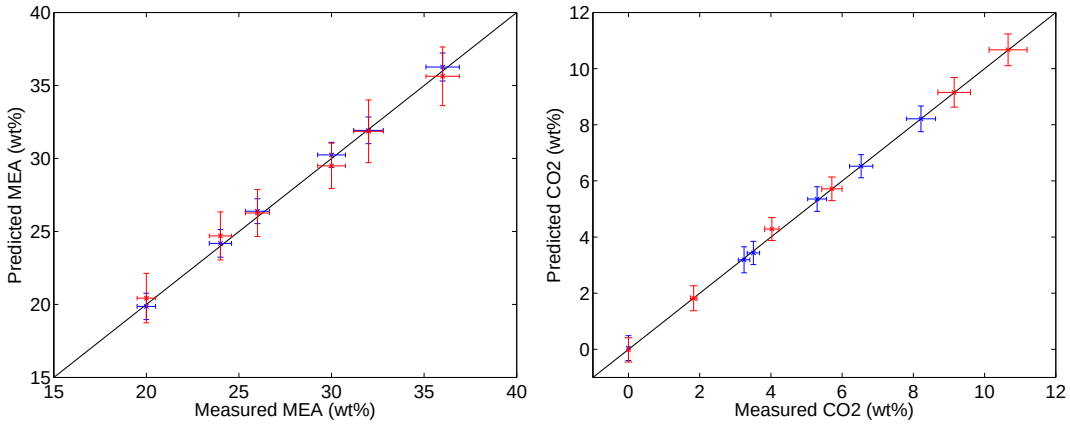

Figure 4-4: Predicted versus measured MEA (left) and CO_2 concentrations for the two temperature levels: 40 [°C] (blue) and 55 [°C] (red)

5 Model validation

Continuous validation tests were carried out at the mini-plant, previously described in Section 3.5. The mini-plant consisted of an absorber and stripper column, for acid gas capturing purposes. Aqueous MEA was used as an absorbent for capturing CO_2 from artificial flue gas. The solvent temperature at the measurement locations was approximately 44 [°C] in the lean circuit and deviated from 32 [°C] to 42 [°C] in the rich circuit due to the changing amount of absorbed CO_2. The acquired data was used as an input to the model calibrated at 40 [°C], described in Section 4.2, and the performance of the model was evaluated. The MEA and CO_2 concentrations in the, during the test runs acquired, samples were predicted using the model based on density, conductivity, refractive index and sonic speed. Only the sonic speed data was not acquired continuously, for reasons described in Section 3.5. Since no continuous sonic speed data was available, the continuous concentrations were evaluated using a model based on density, conductivity and refractive index only. The accuracy of this model was slightly less compared to the model based on four properties (table) but the dynamics in the process were followed.

The continuously predicted concentrations are presented in Figure 4-5. The obtained concentrations in the first run are smooth and dynamics of switching on the CO_2 in the flue gas are well covered. Small fluctuations in the MEA and CO_2 concentrations during the test were caused by changes in the stripper conditions and in the amount of condensate water added. The continuously predicted concentrations for the second run are less smooth. Large fluctuations during the end of the test were caused by the presence of some air bubbles, influencing the measurements. As depicted in Figure 4-1, vaporized water was separated from the stripper outlet gas flow in a condenser. In the mini-plant, this condensate water was recirculated to the system directly after the absorber bottom pump (P1). During the last part of the second test run the condensate water reservoir was almost empty, resulting in the introduction of some air bubbles in the system. The measurement errors caused by these

air bubbles, however, can easily be filtered out of the data and are therefore not much of a problem. The location of condensate water addition also caused the smaller fluctuations during the rest of the test run. The continuous flow of condensate water diluted the solvent to some extent (order of magnitude of 20-30%). A changing solvent flow rate from the absorber bottoms caused changes in the extent of dilution, resulting in the abruptly changing MEA and CO_2 concentrations visible in Figure 4-5. However, the CO_2 step test dynamics were covered accurately. The amount of CO_2 in the flue gas was reduced from 12 [mol%] to 0 [mol%] in six steps, after which it is restored to 12 [mol%] and again switched off and restored to 12 [mol%]. All these events are reported in the figure and well covered by the model.

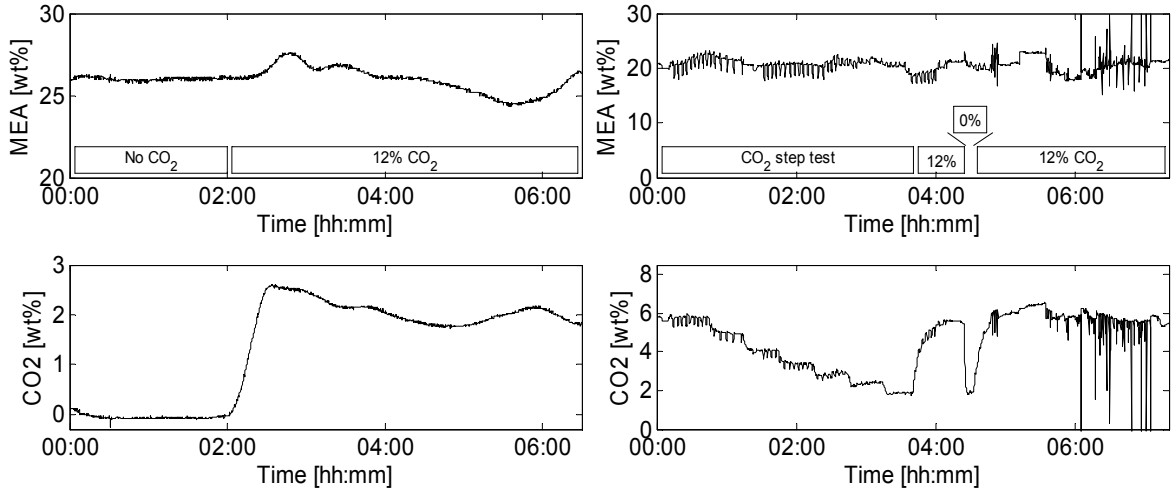

Figure 4-5: Predicted MEA (top) and CO_2 (bottom) concentrations for the first (left) and second (right) continuous test run. Molar CO_2 fractions in the artificial flue gas and the CO_2 step test are given in the top figures.

The accuracy of the predicted MEA and CO_2 concentrations is assessed by analyzing these concentrations in the acquired samples. The measured concentrations were compared to the predicted concentrations based on the, previously mentioned, four analytical techniques. The predictive error was again expressed in terms of the RMSEP, and the results are presented in Table 4-6 for both experiments. The developed method showed to be very accurate, especially for MEA. The use of different density and conductivity measurement apparatus did not disturb the results significantly. Remarkable is the difference in accuracy between both tests. First, it should be noted that the RMSEP for the first experiment was based on only three samples. Furthermore the first run measurements were conducted in the lean flow, which had an almost constant temperature of 44 [°C]. The temperature of the rich flow however, where the measurement loop was installed during the second run, was not controlled at a certain level and fluctuated between 32 [°C] and 42 [°C], resulting in less accurate concentration predictions. Comparison of the RMSEP values for the continuous validation with the lab sample accuracy (Table 4-5 and Table 4-6, respectively) reveals that the continuous accuracy is significantly less compared to the lab sample accuracy, but it is still sufficient for process control purposes. The large deviations in temperature had a limited effect on the predictive performance of the model, but an increased accuracy will be obtained if the measurement loop temperature is maintained at the calibrated level.

Table 4-6: RMSEP values for the continuous trials

	RMSEP MEA [wt%]	RMSEP CO_2 [wt%]
Test run 1	0.46	0.17
Test run 2	0.53	0.31

6 Conclusions and future outlook

A method has been developed to estimate the solvent and solute concentration in the liquid phase of an acid gas chemical absorption process. Density, conductivity, pH, viscosity, sonic speed, refractive index, NIR and UVvis spectroscopy were assessed for their applicability in predictive modeling of the MEA and CO_2 concentration. Based on this first screening, UVvis spectroscopy and viscosity measurements were removed. Evaluation of different combinations of the other analytical techniques resulted in an optimal combination in terms of predictive accuracy and costs, consisting of density, conductivity, refractive index and sonic speed measurements. A multivariate ILS model was calibrated for inline prediction of the solvent and solute concentration. The model was developed using 29 samples with known MEA and CO_2 concentrations. During the continuous tests, the model was able to predict the MEA and CO_2 concentrations with an accuracy of 0.53 and 0.31 [wt%], respectively under changing process conditions. Advantages of the developed model over models based on FTIR data are an increased accuracy, a more than six times reduction in apparatus costs and a simpler installation in actual process plant environment. Expected is that this method is applicable to other solvents in different acid gas capturing processes as well, such as natural gas sweetening.

Future work involves the inclusion of other promising quantities like viscosity for more accurate predictive modeling and model calibration for other industrial processes. Furthermore, process data can be included for increased accuracy reasons as well as an assessment of the extent of solvent degradation. The cyclic loading (or net loading) of the processes can be calculated from process data and compared to the cyclic loading based on model predictions. Process data can also be used to compare theoretical absorbing and desorbing behavior with actual plant performance to assess the influence of solvent degradation on plant performance. Another interesting option is increasing the robustness of the model, by including some degradation or contamination into the calibration set. In actual process plant operation this can be advantageous because prolonged plant operation results in more solvent degradation and pollution. Increased model robustness to degradation and contamination of the model will therefore increase its applicability in industrial process operation.

Measurement of the density, conductivity, refractive index and sonic speed, combined with a multivariate chemometric method can readily be used to accurately monitor the liquid MEA and CO_2 concentrations in a post-combustion CO_2 capturing process.

Chapter 5

Model robustness

For actual process plant application, model robustness against solvent degradation is of major importance. Solvent degradation influences the measurements, thereby affecting the predictive accuracy of the model. In this section the robustness of the model against solvent degradation is assessed. Offline model robustness was evaluated based on pilot plant samples from the 2012 CATO-2 campaign. Online analysis was carried out at the TNO microplant, during a continuous experiment lasting three weeks. First, the previously described model calibration was extended with degraded samples, aimed at increasing the robustness of the model against disturbances.

5-1 Model calibration with degraded samples

For increased robustness purposes the calibration set was extended with eight degraded MEA samples. Four degraded samples were added to the validation set. These samples were taken from a series of experiments in the Octavius project, aimed at assessment of the influence of metals on oxidative MEA degradation. Three different degraded samples were used. The first was degraded without any further external contamination, to the second some stainless steel was added and the third contained a small amount of fly ash. Different amounts of degraded MEA samples were added to a subset of the calibration samples and were used as calibration samples themselves. Expected is that these samples contain a collection of degradation products representative for industrial applications. The MEA and CO_2 concentration of these polluted samples is measured using the previously described HCL titration and boiling phosphoric acid methods respectively (Sections 3-3-9 and 3-3-10). Table 5-1 shows the polluted samples and the amount of pollution added. All samples have been measured both at 40 and 55 [°C].

In accordance with the development of the unpolluted models, PLS models were built based on these polluted data sets and the model performance was evaluated using the validation sample set, extended with the polluted validation samples. The RMSEP values for both MEA and CO_2, at both temperature levels, were obtained and are listed in Table 5-2.

Comparison of these results with the RMSEP for the unpolluted model (as listed in Table 4-4) shows that the polluted models are less accurate, due to the addition of polluted samples to

Table 5-1: Pollution added to calibration and validation samples

Sample	Amount of sample (g)	Poll sample 1 [g]	Poll sample 2 [g]	Poll sample 3 [g]
#5	25.00	5.00	5.00	5.00
#8	29.94	5.00	0	0
#9	30.00	0	0	10.00
#10	30.00	0	5.00	0
#13	30.00	10.00	0	0
#T1	30.00	7.50	0	0
#T4	30.00	0	10.00	0
#T11	30.00	5.00	5.00	5.00
#T13	30.00	0	0	7.50

Table 5-2: RMSEP values for the developed models for 40 [°C] (left) and 55 [°C] (right)

Included data	RMSEP MEA [wt%]	RMSEP CO_2 [wt%]
All	0.47/0.64	0.38/0.26
NIR	0.59/0.91	0.48/0.29
1^{st} derivative of NIR	0.58/0.57	0.47/0.24
2^{nd} derivative of NIR	0.50/0.58	0.42/0.29
Density/pH/cond./refr. ind./sonic speed	0.51/0.74	0.24/0.28
Density/cond./refr. ind./sonic speed	0.46/0.67	0.23/0.23
Density/refr. ind./sonic speed	0.46/1.06	0.28/0.27
Density/pH/refr. ind./sonic speed	0.45/1.05	0.27/0.29
FTIR *(obtained by Geers et al.)*[8]	0.38	0.26

the validation set. However, the difference between the calibration for 40 and 55 [°C] is smaller for the polluted models. This indicates that the polluted model is more robust to disturbances in the validation set and is better able to cope with the effects of heating the samples to 55 [°C], described in Section 4-2. The RMSEP for the unpolluted, 40 [°C] model, if the same polluted validation set is used, is 0.71 [wt%] and 0.48 [wt%] for MEA and CO_2 respectively. Therefore, in case the polluted validation data set is used, the polluted model performs significantly better than the unpolluted model. The combination of density, conductivity, refractive index and sonic speed data, which was chosen as favourable combination for the unpolluted model, is the most accurate for both MEA and CO_2 at both temperature levels.

5-2 Pilot samples

The influence of degradation components on the accuracy of both the polluted and clean model was first tested on pilot plant samples, obtained during a campaign in 2012. In 2008, TNO commissioned a CO_2 capture plant, able to process approximately 1500 [Nm^3/h] flue gas and to capture 250 [kg/h] of CO_2. Several experimental campaigns were carried out at this pilot plant in 2012, as a part of the CATO-2 research program. Eleven during those campaigns obtained samples were analyzed in the lab to acquire model input data (density, conductivity, refractive index and sonic speed) and the MEA and CO_2 concentrations were analyzed. The measured concentrations were subsequently compared to the predicted concentrations, in

Table 5-3: RMSEP for MEA and CO_2 of pilot samples

	RMSEP MEA [wt%]	RMSEP CO_2 [wt%]
Unpolluted model	0.75	0.29
Polluted model	0.94	0.26

order to evaluate the model accuracy for these degraded samples and to study the effects of degradation on this accuracy. This was solely done for the model calibrated at 40 [°C]. The RMSEP for both the unpolluted and the polluted model are presented in Table 5-3.

The RMSEP for the polluted model is, opposed to what was found in Section 5-1, notably larger for MEA. This indicates that the degradation products that were included in the model do not match the degradation products in the pilot plant samples. As mentioned in Section 5-1 the added degraded samples included mainly oxidative degradation products that were generated at low temperature. In the pilot plant, the solvent has been at higher temperatures and pressures (at stripper conditions) and, therefore, not only oxidative degradation did occur, but carbamate polymerization as well. Furthermore, real flue gasses were treated in the pilot plant, containing contaminants that were also causing degradation. The pilot samples contained another 'degradation product mix' than the Octavius samples, causing a larger predictive error in the polluted model. The amount of degradation in the pilot samples could not be identified accurately, but it ranged between the 2 and 7 [%] of the initial MEA concentration. It is evident that even the polluted pilot samples from an experiment that had more than 1000 operating hours were still accurately monitored by both models.

5-3 Microplant experiment

For further robustness assessment purposes a continuous experiment was carried out at the previously described microplant (Section 3-2). The experiment lasted approximately three weeks and was aimed at an assessment of the influence of gradual degradation on the model performance. Degradation was increased by using a mixture of air and CO_2 as flue gas, having a O_2 concentration of around 17.6 [vol%]. Furthermore, during the last days of the experiment, coppersulfate was added, which has a catalytic effect on oxidative degradation. Density, conductivity, refractive index and sonic speed were measured online in a temperature controlled test rig. The temperature of this measurement loop was maintained at approximately 40 [°C]. The continuous results and the analyzed samples that were taken are depicted in Figure 5-1. These results were obtained using the unpolluted model. The continuous results obtained using the polluted model are depicted in Appendix C-3. RMSEP values for both models are listed in Table 5-4.

Table 5-4: RMSEP for MEA and CO_2 during the microplant experiment

	RMSEP MEA [wt%]	RMSEP CO_2 [wt%]
Unpolluted model	0.75	0.18
Polluted model	0.57	0.23

The polluted model performs significantly better when it comes to MEA, and slightly worse for CO_2. Since MEA is the degrading component, it was expected that the addition of pollution to the model would have the strongest effect on the predicted MEA concentration.

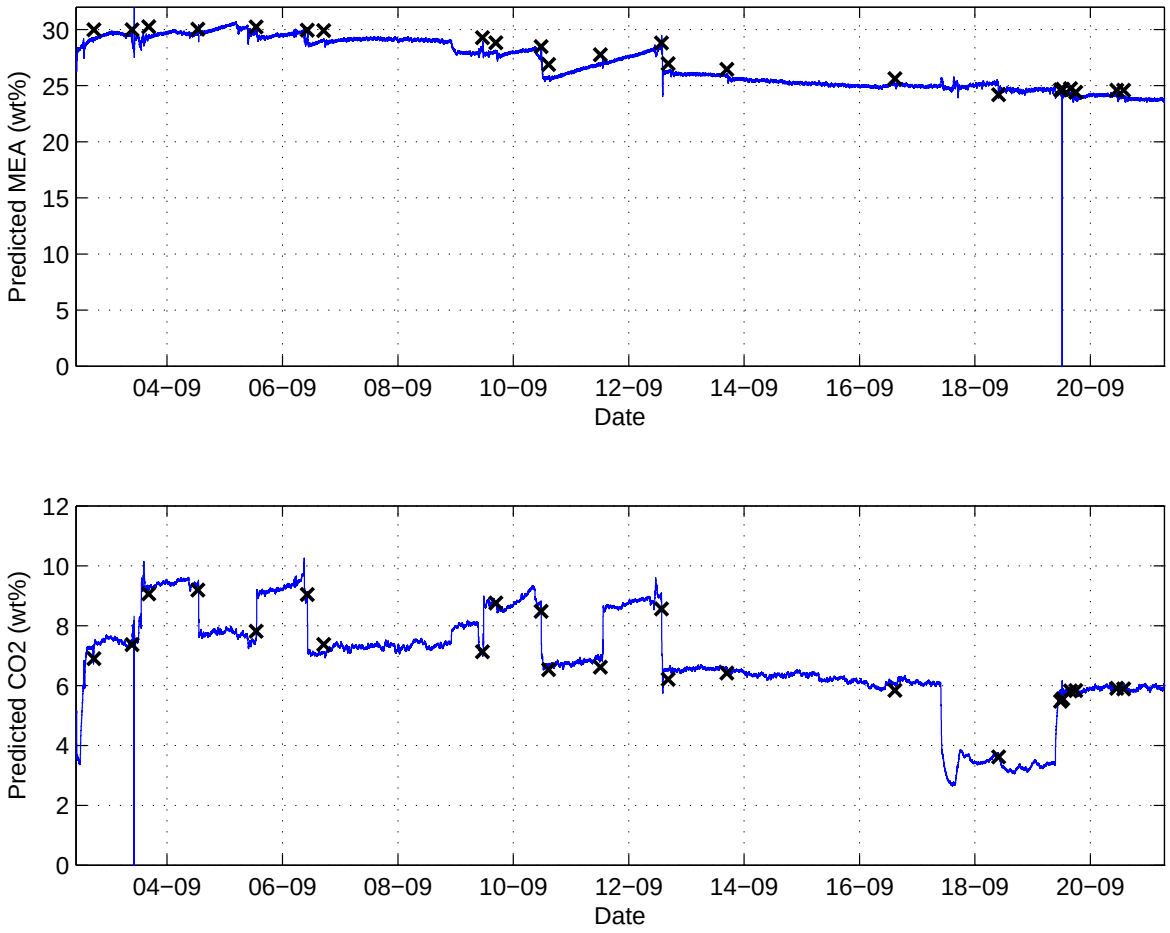

Figure 5-1: Continuously predicted MEA and CO_2 concentrations and the concentrations in analyzed samples (marks) during the microplant experiments, obtained with the unpolluted model

The RMSEP for the microplant experiment is comparable with the results obtained during the KIT experiments, in case the same unpolluted model is used. The RMSEP for MEA is a bit higher whereas the RMSEP for CO_2 is lower. These differences were caused by a slightly different conductivity probe calibration and by the use of a different sonic speed probe. Notwithstanding the differences in the model accuracy, it still predicts the MEA and CO_2 concentrations within an error of 0.75 and 0.23 [wt%] for MEA and CO_2 respectively.

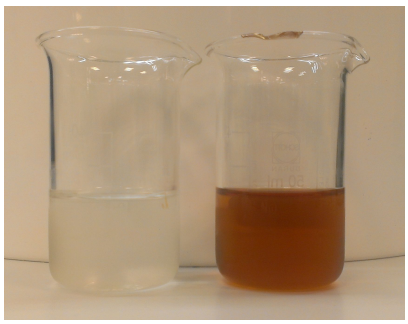

Figure 5-2: Changed colour of the samples between the beginning and the end of the microplant experiment

The continuous predictions of the MEA concentration reveal a reduction from the initial 30 [wt%] to below 25 [wt%]. This reduction is partly caused by sampling. Due to the limited liquid volume in the microplant (around 8 [l]), the replacement of the sample volume by water dilutes the solvent substantially. 24 samples of around 40 [ml] each were taken, adding up to a total sample amount of 0.96 [l]. The remaining reduction in MEA concentration (around 8.5 %)

is caused by degradation of the solvent. The solvent colour is an indication of the amount of degradation and the change in colour between the first and the last sample is depicted in Figure 5-2.

Since the test rig was switched between the lean and rich stream several times, some step changes in the CO_2 concentrations are visible in Figure 5-1. The period with a CO_2 concentration between 3 and 4 [wt%] is caused by a reduced CO_2 content in the flue gas during that period.

There seems to be no relation between the error in the predicted concentrations and the amount of degradation, as can be seen in Figure 5-3. The error does not grow over time, indicating that the model is able to predict the MEA and CO_2 concentrations even in degrading circumstances.

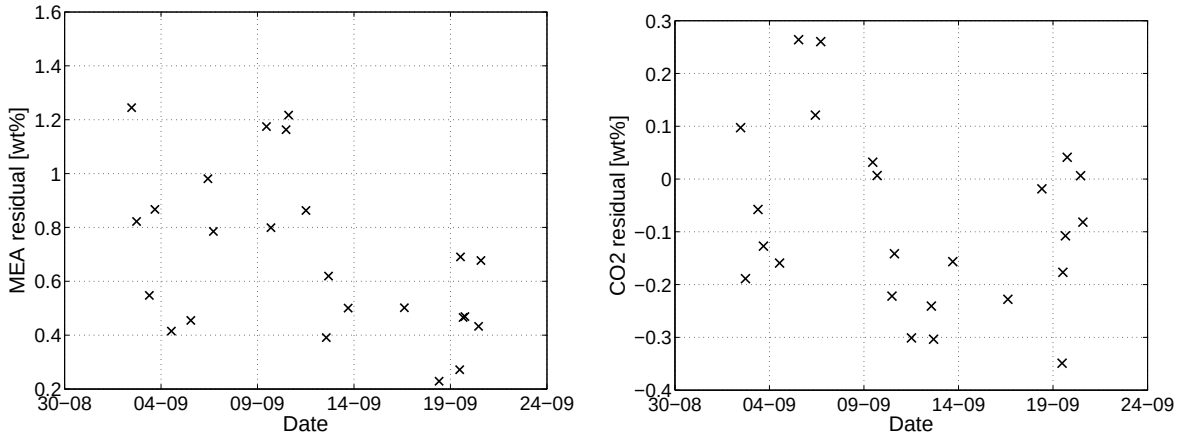

Figure 5-3: Error in MEA and CO_2 estimations over time. No significant relation between the error and the time of operation was visible.

Chapter 6

Process data

The availability of online data concerning Monoethanolamine (MEA) and CO_2 concentrations enables new ways to evaluate the performance of the absorption process. The combination of the model with process data that is already measured is one of these possibilities. This combination can be used for model and process performance evaluation, which will both be treated in this chapter.

6-1 Cyclic loading

The first and most straightforward method to combine process data with online MEA and CO_2 concentrations is by comparing the cyclic loading. The cyclic loading is the difference between the lean and rich loading and is calculated from process data by dividing the amount of captured CO_2 by the MEA flow rate:

$$\alpha_{cyc} = \alpha_{rich} - \alpha_{lean} = \frac{\dot{n}_{CO_2,cap}}{\dot{n}_{MEA}} \tag{6-1}$$

The cyclic loading is in this case expressed in terms of the net loading of MEA, but it can also be expressed in terms of the entire flow rate in the lean or rich stream. The amount of CO_2 captured from the flue gas can either be calculated from the difference between CO_2 concentration in the gaseous in- and out-let of the absorber or by the difference between the CO_2 concentration in the rich and lean flow. This gives two ways to obtain the cyclic loading and the results can be compared to evaluate the predictive performance of the model and to identify possible model runaways. This possibility has not been assessed experimentally. In order to do so, two measurement loops are required (both in the lean and rich stream) and there was only one loop available.

6-2 Vapour-Liquid-Equilibria

Another way to exploit the available process data is to compare the theoretical and actual Vapour Liquid Equilibrium (VLE) of the MEA-H_2O-CO_2 system. Based on pressures and

temperatures in the absorber and stripper the theoretical rich and lean loading can be determined. The theoretical loadings are then compared to the actual loadings obtained by the chemometric model and the deviations from the theoretical behaviour are assessed. The actual VLE will never reach the theoretical values due to non-ideal column performance and due to the fact that the columns (especially the absorber column) is not reaching equilibrium. However, degradation will cause a further deviation from the theoretical behaviour and that increased deviation can be considered as a measure for the amount of solvent degradation and deactivation. It is therefore very useful in process control.

Experimental VLE data for the MEA-H_2O-CO_2 system as a function of the partial pressure of CO_2 and the temperature has been fitted by Oexmann [40]. The CO_2 loading appeared to be almost unaffected by the MEA concentration for loadings lower than 0.5 [mole/mole MEA]. It can, therefore, be expressed as a function of the temperature and the partial pressure of CO_2 only:

$$\ln P^*_{CO_2} = C_{pCO_2,0} + C_{pCO_2,1}\frac{1}{T} + C_{pCO_2,2}\alpha + C_{pCO_2,3}frac\alpha T + C_{pCO_2,4}\alpha^2 + C_{pCO_2,5}\frac{\alpha^2}{T} + C_{pCO_2,6}\alpha^3 + C_{pCO_2,7}\frac{\alpha^3}{T} + C_{pCO_2,8}\alpha^4 \tag{6-2}$$

This equation has been fitted to experimental data by Oexmann and appeared to be more accurate than the electrolyte-NRTL equation of state developed by Austgen et al.[41]. Experimental data is covered more accurately by the Oexmann equation, especially in the high loading regime (above 0.45 [mole/mole MEA]). The only required process data is the partial pressure of CO_2 and the temperature at the liquid outlet of both the absorber and stripper column. Temperatures can directly be obtained from the process data, but the partial pressures of CO_2 have to be calculated. Using the absorber top pressure, the absorber pressure drop and the CO_2 content at the gaseous absorber inlet, the partial pressure of CO_2 at the absorber liquid outlet was calculated. Obtaining the partial pressure of CO_2 at the stripper liquid outlet is more complicated. The total pressure is easily found using the stripper top pressure and the pressure drop over the stripper. The CO_2 partial pressure is obtained by subtracting the partial pressure of H_2O at stripper bottom conditions from the total pressure at that location. The relation between the partial pressure of H_2O and the solvent temperature has been fitted from data obtained using Aspen 8.0 and the electrolyte NRTL - Redlich Kwong thermodynamic model. The fitted equation was of the form of the Antoine equation, which provided good fits for the MEA-H_2O system:

$$\log(P_{H_2O}) = A - \frac{B}{T_{str}} \tag{6-3}$$

A and B are fitted parameters and a function of the MEA concentration in the stripper. These parameters were fitted to the MEA concentration using a second order polynomial fit. The fitted values are reported in Appendix D.

A performance parameter β was defined as the ratio between the actual and theoretical CO_2 loading:

$$\beta = \frac{\alpha_{act}}{\alpha_{theor}} \tag{6-4}$$

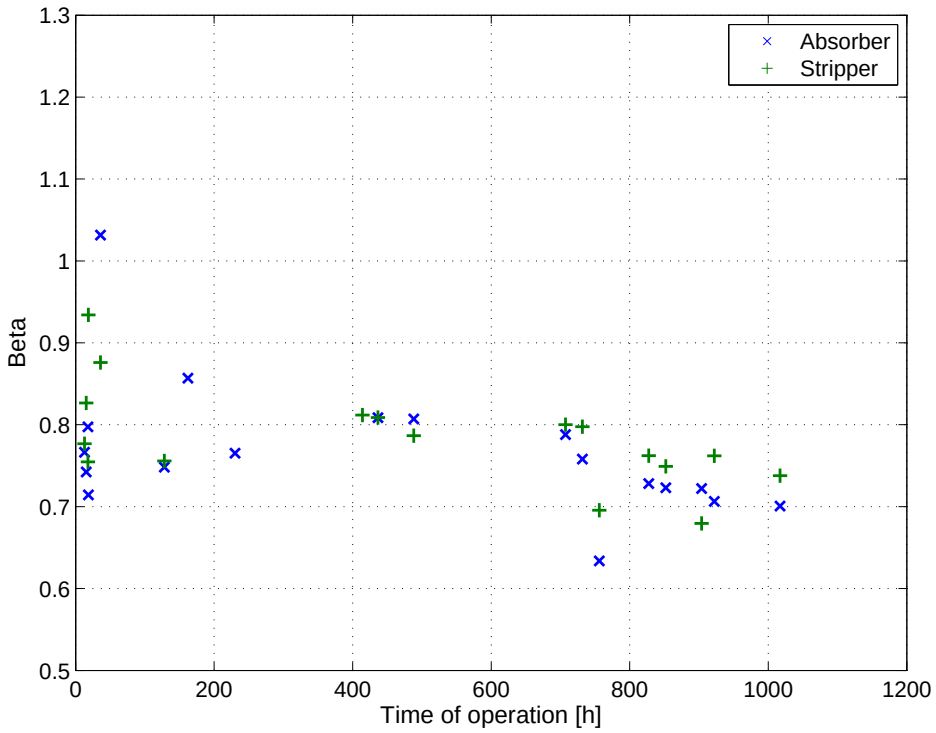

Figure 6-1: Performance parameter β during the 2012 pilot plant campaign

Since in the absorber column equilibrium will generally not be reached, β will always be smaller than one. The stripper is operating closer to equilibrium and β will therefore be larger under stripper conditions, as compared to the absorber.

A first test of this performance parameter β was carried out using pilot plant data from the same campaign as used in Section 5-2. Process data from that campaign, together with available MEA and CO_2 concentrations from the taken samples, was used to calculate the theoretical loading and the resulting values for β are depicted in Figure 6-1.

For both the stripper and absorber, β seems to be slightly decreasing over time, but the decreasing trend is very noisy and therefore not suitable as indicator for the amount of solvent degradation. Better results would probably be obtained if an experiment was carried out without any solvent reclaiming and addition of fresh solvent. Several refills with fresh solvent were done during the 2012 campaign, disturbing the obtained results. During the last part of the experimental campaign (starting from 600 [h] of operation) no further refills were performed and the decreasing trends in β for both the absorber and stripper are indeed more obvious.

Chapter 7

Conclusions and future outlook

7-1 Conclusions

A method has been developed for online monitoring of the MEA and CO_2 concentrations in a chemical absorption PCC process. Density, conductivity, pH, refractive index, sonic speed and viscosity measurements, as well as NIR and UVvis spectroscopy have been assessed for their applicability as indicators of the MEA and CO_2 concentrations in the solvent. Based on this first screening, viscosity and UVvis spectroscopy have been removed from the data set and model calibration has been done using the remaining analytical techniques. An optimal combination of calibration data has been chosen, based on predictive accuracy of the developed models and the costs of the required measurement apparatus. A combination of density, conductivity, refractive index and sonic speed measurements was found to be favourable over the other combinations. This data set was used as input for a multivariate ILS model, that calculates the MEA and CO_2 concentrations of the measured solvent. The method was demonstrated at a CO_2 capturing miniplant and during a three week experiment at a microplant. The method is applicable within its calibration range: 20-36 [wt%] for MEA (with respect to the unloaded solution) and a CO_2 loading of 0-0.5 mole per mole MEA, and at two temperature levels: 40 and 55 [°C]. The model calibrated at 40 [°C] has been validated extensively at both the mini- and microplant and the mean predictive error in the validation experiments always stayed within 0.94 [wt%] and 0.31 [wt%] for MEA and CO_2 respectively. The best accuracy was obtained during the offline lab sample validation and was 0.24 [wt%] for MEA and 0.05 [wt%] for CO_2. The inclusion of degraded samples in the calibration set had a positive influence on the predictive accuracy of the model in degrading circumstances if the added pollution was of a comparable nature as the degradation in the predicted solvent. In case the solvent degradation is of another nature the addition of degraded samples to the calibration set had a negative effect on the predictive accuracy of the model.

The combination of process data with the model provides new insight in model and process performance. Two ways to do so were identified. Comparison of the cyclic loading calculated from the model and from the process data provides a measure for the model performance. This has not experimentally been tested due to the lack of a double test loop. Another option to combine process data with the model is a comparison of the actual and theoretical VLE in the absorber and stripper liquid outlet to derive a degradation parameter. This was tried

for the pilot samples from 2012, but no significant relation between the derived degradation parameter and the time of operation was found.

Advantages of the developed method over the previously investigated method based on FTIR measurements[8, 9] are an increased accuracy, a more than six fold reduction in apparatus costs, a simpler installation in process plants and an increased robustness against unwanted (degradation) components. The robustness with respect to degradation has been assessed at the microplant during a three week continuous experiment and no significant relation between the amount of degradation and the predictive accuracy of the model was found. The accuracy of the model was retained, with around 8.5 [%] of the MEA being degraded. Furthermore, the method showed good robustness to temperature differences (it was still accurate with temperature fluctuations of 10 [°C]) and to the use of different analytical apparatus to collect the measurement data.

The model provides new possibilities from a process control and a scientific perspective. The chemical absorption process can be accurately monitored and can therefore better be controlled by e.g. solvent reclaiming and alterations in process conditions. From a scientific perspective, the continuous monitoring of the MEA and CO_2 concentrations gives a more detailed insight in process behaviour and in the influence of different parameters on process performance.

The developed method is believed to be applicable in other acid gas capturing processes as well, such as natural gas sweetening. The applications are therefore numerous and the potential of the developed method is promising.

7-2 Future outlook

Future work should involve an attempt to increase the predictive accuracy and robustness of the model. This can be done via a more detailed assessment of other promising solvent properties like viscosity, for model calibration. Inclusion of other solvent properties might increase the robustness of the model to e.g. solvent degradation.

This model robustness can also be increased by the addition of a more complete degradation products mix to the calibration samples to increase the accuracy for degraded solvents. This study pointed out that, if the added degradation products were of the same nature as the degradation in the measured solvent the model accuracy was increased. Addition of a representative degradation mix for industrial applications would increase the applicability of the model in process plants.

Furthermore, the applicability of the developed model in other (acid gas capturing) industrial processes has to be investigated, for the model having a large potential in other processes and industries.

Another very interesting option is a more extensive assessment of the combination of process data with the developed model. The two possibilities investigated in this study should be verified experimentally and other possibilities could be developed. To calculate the cyclic loading from process data, a second measurement loop is required. For the evaluation of the actual vs. theoretical VLE a gradual degradation experiment has to be carried out at the miniplant or at a pilot plant, with accurate monitoring of the process conditions.

Appendix A

A-1 PID microplant

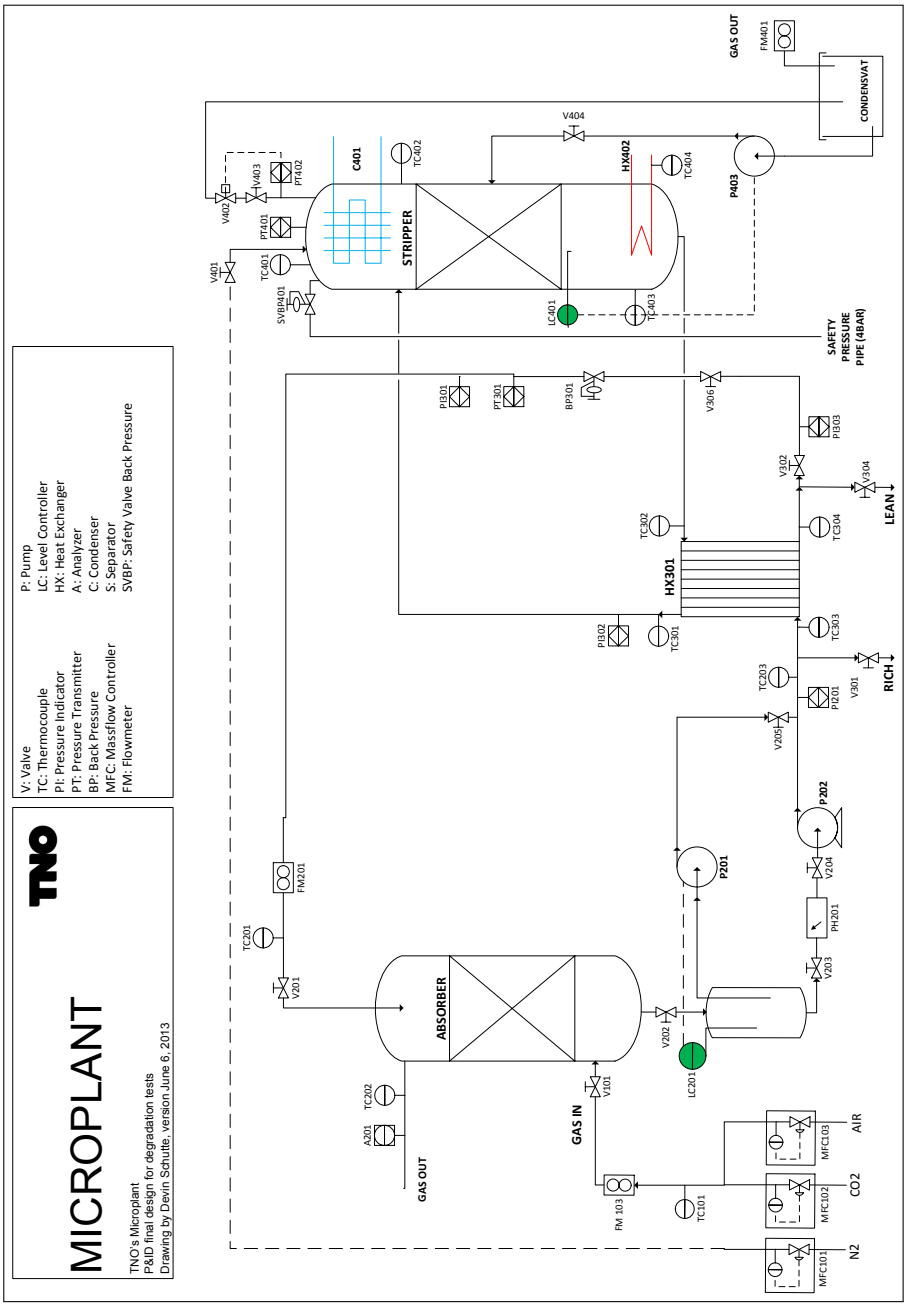

A-2 PID miniplant

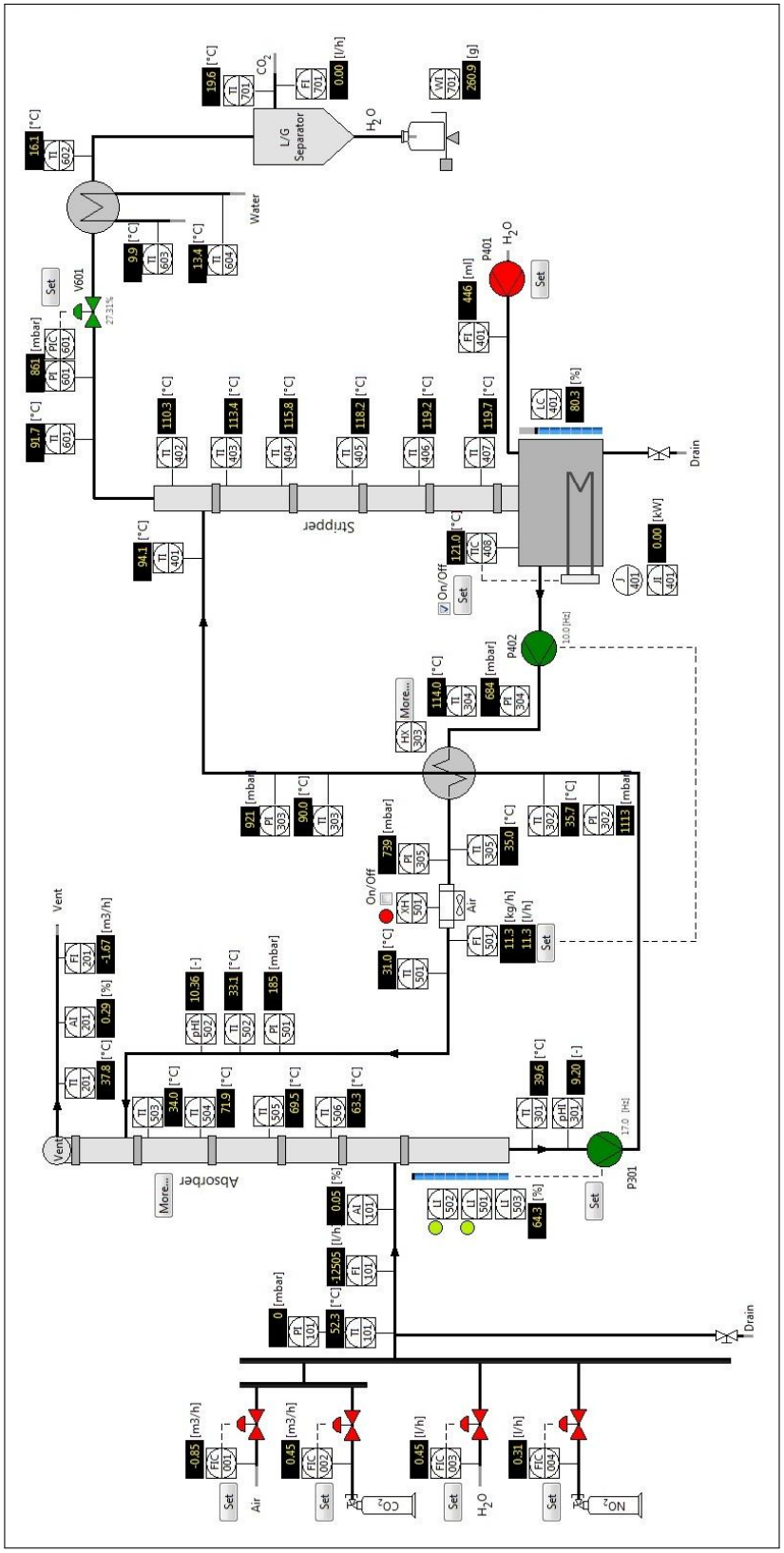

Appendix B

B-1 Screening experiments

Table B-1: Overview of the high (1) and low (-1) values for the samples used in the screening experiments

Sample	MEA	CO_2	HNO_3	H_2SO_4	HEIA	Pollutants	Temperature
#1	0	0	0	0	0	0	0
#2	1	1	1	1	1	1	1
#3	1	1	1	1	-1	-1	-1
#4	1	1	-1	-1	-1	-1	1
#5	1	1	-1	-1	1	1	-1
#6	1	-1	1	-1	-1	1	1
#7	1	-1	1	-1	1	-1	-1
#8	1	-1	-1	1	1	-1	1
#9	1	-1	-1	1	-1	1	-1
#10	-1	1	1	-1	1	-1	1
#11	-1	1	1	-1	-1	1	-1
#12	-1	1	-1	1	-1	1	1
#13	-1	1	-1	1	1	-1	-1
#14	-1	-1	1	1	-1	-1	1
#15	-1	-1	1	1	1	1	-1
#16	-1	-1	-1	-1	1	1	1
#17	-1	-1	-1	-1	-1	-1	-1

Table B-2: Raw measurement data from screening experiments

Sample	Density [g/ml]	Conductivity [mS/cm]	pH -	Refr. ind. [n_D20]	Viscosity [mpa.s]	Speed of sound [m/s]
#1	1.0455	20.07	10.14	1.382	2.695	1698.9
#2	1.0769	29.65	9.33	1.404	2.447	1760.8
#3	1.0869	22.31	10.54	1.396	5.770	1757.8
#4	1.0502	20.12	9.62	1.394	1.913	1746.6
#5	1.0820	19.30	10.56	1.398	5.151	1786.8
#6	1.0096	14.57	10.01	1.386	1.854	1713.2
#7	1.0248	5.25	11.43	1.379	3.362	1725.2
#8	1.0065	5.82	10.32	1.381	1.502	1721.1
#9	1.0345	10.85	10.98	1.383	3.649	1725.4
#10	1.0563	32.45	9.25	1.383	1.573	1690.6
#11	1.0820	34.75	10.02	1.384	3.017	1712.0
#12	1.0660	38.80	9.07	1.386	1.531	1713.5
#13	1.0790	26.98	10.26	1.383	3.001	1707.3
#14	1.0066	15.50	9.98	1.367	1.159	1653.3
#15	1.0372	21.24	10.69	1.372	2.437	1684.6
#16	1.0026	12.36	10.05	1.369	1.198	1667.5
#17	1.0111	0.87	12.24	1.363	2.137	1646.0

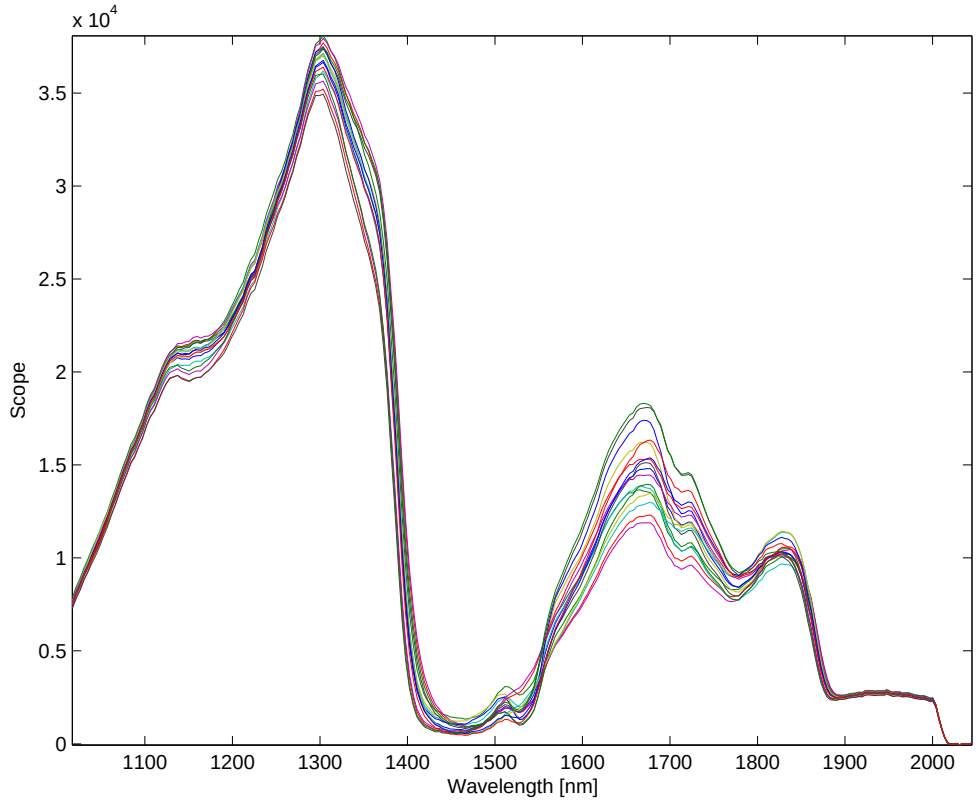

Figure B-1: Raw NIR spectra for the seventeen samples used in the screening experiments, each line representing an individual spectrum

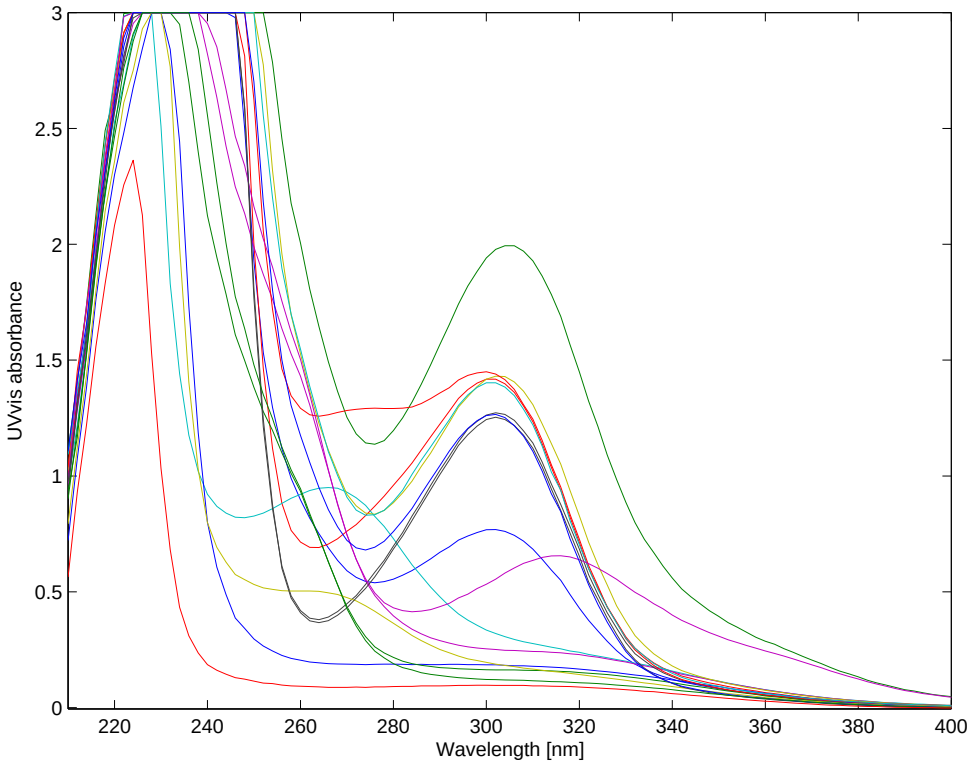

Figure B-2: Raw UVvis absorbance spectra for the seventeen samples used in the screening experiments, each line representing an individual spectrum.

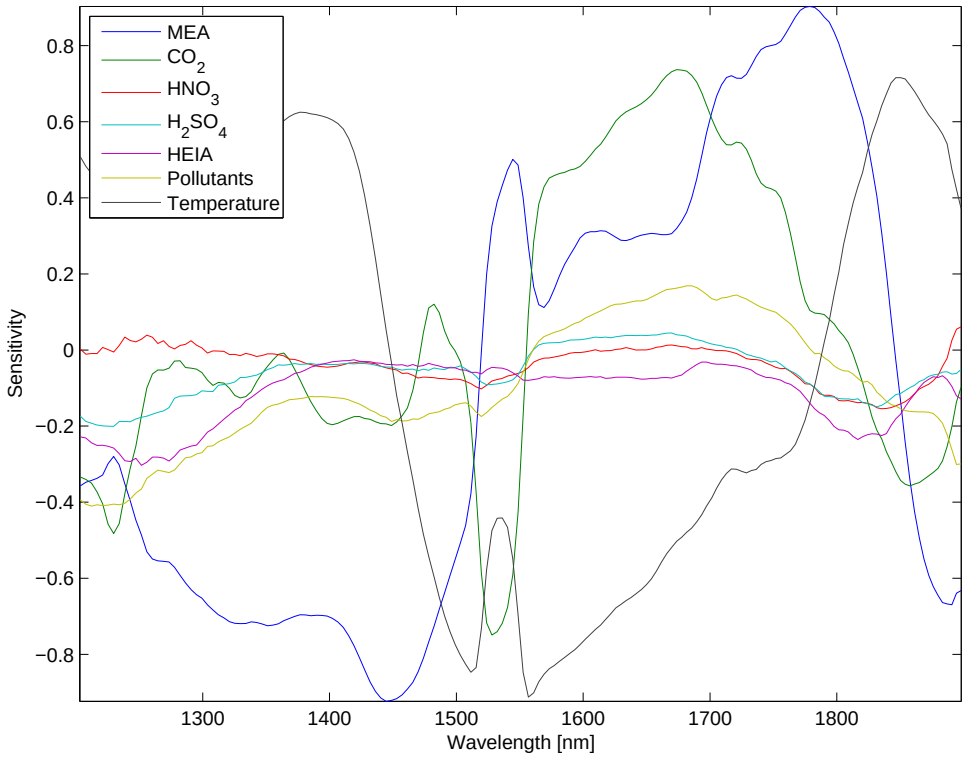

Figure B-3: Sensitivity results for the entire NIR spectrum

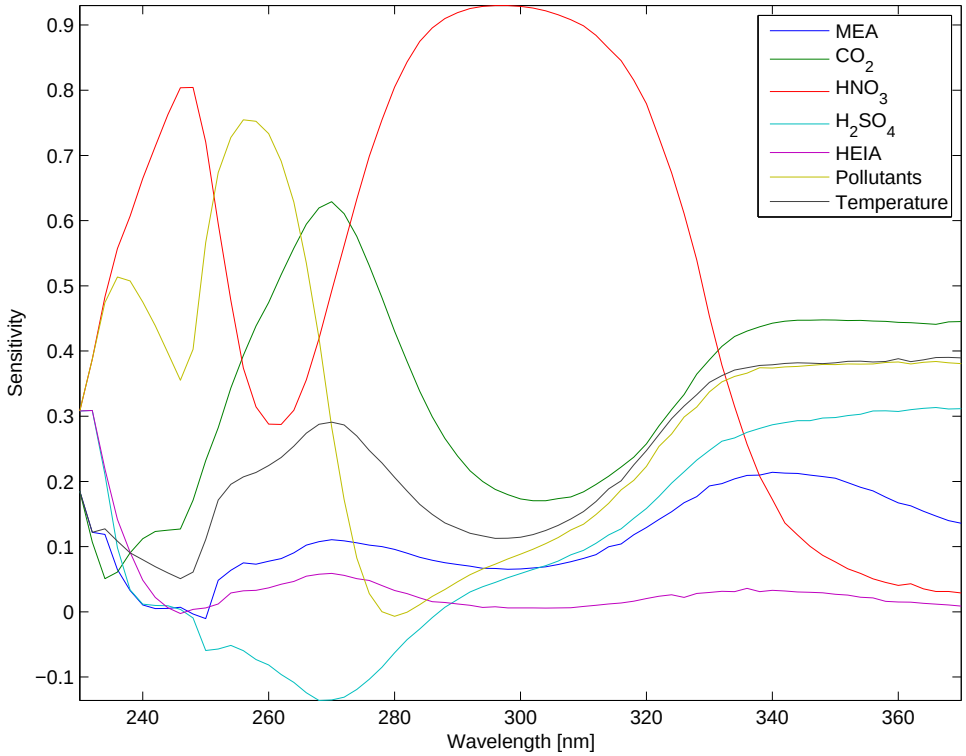

Figure B-4: Sensitivity results for the entire UVvis spectrum

B-2 Model calibration

Table B-3: Raw data used in final model calibration at 40 [°C]. #C are the calibration and #V the validation samples

Sample	MEA [wt% unl. solv.]	CO_2 [wt%]	Density [g/ml]	Conductivity [ms/cm]	Refr. ind. [n_D20]	Son speed [m/s]
#C1	20	0.0	1.001	1.67	1.357	1624.0
#C2	20	3.6	1.036	28.58	1.366	1654.3
#C3	20	6.9	1.069	46.60	1.374	1678.9
#C4	24	2.2	1.023	17.75	1.367	1661.3
#C5	24	4.3	1.044	28.84	1.373	1677.1
#C6	24	6.3	1.064	39.50	1.378	1694.0
#C7	28	0.0	1.004	1.16	1.367	1661.4
#C8	28	2.5	1.028	29.02	1.373	1684.8
#C9	28	5.0	1.052	29.25	1.380	1700.7
#C10	28	7.3	1.075	39.45	1.385	1719.0
#C11	28	9.5	1.096	46.65	1.391	1736.1
#C12	32	2.9	1.034	17.02	1.380	1704.1
#C13	32	5.6	1.060	28.62	1.387	1723.1
#C14	32	8.2	1.086	36.35	1.393	1745.9
#C15	36	0.0	1.007	0.91	1.378	1694.6
#C16	36	6.3	1.068	26.89	1.393	1744.0
#C17	36	11.8	1.123	35.50	1.406	1792.2
#V1	20	5.3	1.053	39.85	1.370	1666.9
#V2	24	8.2	1.083	37.45	1.383	1707.4
#V3	26	3.5	1.037	18.51	1.374	1681.9
#V4	30	6.5	1.068	26.39	1.386	1723.0
#V5	32	0.0	1.006	0.77	1.373	1679.1
#V6	36	3.2	1.038	12.72	1.386	1725.5

Table B-4: Raw data used in final model calibration at 55 [°C]. #C are the calibration and #V the validation samples

Sample	MEA [wt% unl. solv.]	CO_2 [wt%]	Density [g/ml]	Conductivity [ms/cm]	Refr. ind. [n_D20]	Son speed [m/s]
#C1	20	0.0	0.993	2.26	1.357	1624.9
#C2	20	3.6	1.028	38.70	1.367	1658.0
#C3	20	6.9	1.061	60.40	1.375	1683.5
#C4	24	2.2	1.016	22.96	1.368	1660.5
#C5	24	4.3	1.036	39.10	1.374	1678.2
#C6	24	6.3	1.057	52.75	1.381	1704.1
#C7	28	0.0	0.996	1.59	1.368	1654.7
#C8	28	2.5	1.020	39.75	1.376	1682.3
#C9	28	5.0	1.044	39.00	1.380	1696.8
#C10	28	7.3	1.067	51.50	1.386	1718.5
#C11	28	9.5	1.088	62.50	1.392	1737.8
#C12	32	2.9	1.025	22.64	1.382	1696.0
#C13	32	5.6	1.052	38.25	1.389	1719.4
#C14	32	8.2	1.078	50.65	1.395	1743.5
#C15	36	0.0	0.999	1.32	1.379	1679.9
#C16	36	6.3	1.059	37.15	1.394	1736.2
#C17	36	11.8	1.114	50.25	1.409	1798.1
#V1	20	1.8	1.011	13.74	1.362	1642.3
#V2	24	0.0	0.995	1.11	1.364	1642.1
#V3	26	5.7	1.051	29.00	1.380	1699.7
#V4	30	4.0	1.038	21.2	1.381	1696.9
#V5	32	10.7	1.102	36.95	1.399	1761.5
#V6	36	9.1	1.088	30.15	1.401	1760.6

B-3 Model validation

Table B-5: Measurement results for the samples acquired during the first continuous validation run at KIT

Sample	MEA [wt% unl. solv.]	CO_2 [wt%]	Density [g/ml]	Conductivity [mS/cm]	Refr. ind. [n_D20]	Sonic speed [m/s]
#1.1	27.7	2.6	1.027	20.36	1.373	1683.2
#1.2	25.7	2.3	1.023	18.78	1.370	1674.0
#1.2	26.2	2.0	1.021	17.24	1.370	1671.2

Table B-6: Measurement results for the samples acquired during the second continuous validation run at KIT

Sample	MEA [wt% unl. solv.]	CO_2 [wt%]	Density [g/ml]	Conductivity [mS/cm]	Refr. ind. [n_D20]	Sonic speed [m/s]
#2.1	21.7	5.4	1.059	35.16	1.374	1680.5
#2.2	20.7	4.5	1.050	32.58	1.372	1672.1
#2.3	20.4	3.7	1.041	29.26	1.368	1660.5
#2.4	20.4	3.1	1.034	24.90	1.366	1657.4
#2.5	22.4	2.7	1.030	20.92	1.366	1656.9
#2.6	22.1	2.2	1.025	16.91	1.365	1655.5
#2.7	19.5	1.5	1.019	13.00	1.362	1637.2
#2.8	21.2	5.4	1.054	36.38	1.372	1675.3
#2.9	19.8	5.7	1.057	42.28	1.370	1670.0

Appendix C

C-1 Polluted model calibration

Table C-1: Raw data used in polluted model calibration at 40 [°C]. #P are the polluted calibration and #PV the polluted validation samples

Sample	MEA	CO_2	Density	Conductivity	Refr. ind.	Sonic speed
[wt% of unl.	solv.]	[wt%]	[g/ml]	[mS/cm]	[n_D20]	[m/s]
#P1	22.20	4.99	1.058	37.35	1.377	1685.5
#P2	27.00	3.16	1.060	35.70	1.381	1704.6
#P3	25.60	5.16	1.061	34.55	1.381	1702.1
#P4	26.70	7.07	1.080	43.05	1.386	1722.2
#P5	29.30	5.93	1.072	34.00	1.390	1730.4
#P6	21.10	6.82	1.079	45.30	1.383	1697.2
#P7	18.70	5.94	1.070	46.45	1.379	1680.0
#P8	18.20	5.74	1.069	46.20	1.378	1678.0
#PV1	20.20	5.60	1.061	47.95	1.374	1675.1
#PV2	27.20	6.39	1.074	42.80	1.386	1717.9
#PV3	26.40	4.74	1.059	34.20	1.382	1702.2
#PV4	32.40	8.47	1.097	42.55	1.397	1757.6

Table C-2: Raw data used in polluted model calibration at 55 [°C]. #P are the polluted calibration and #PV the polluted validation samples

Sample	MEA	CO_2	Density	Conductivity	Refr. ind.	Sonic speed
[wt% of unl.	solv.]	[wt%]	[g/ml]	[mS/cm]	[n_D20]	[m/s]
#P1	22.20	4.99	1.051	50.45	1.378	1686.7
#P2	27.00	3.16	1.052	45.25	1.382	1700.4
#P3	25.60	5.16	1.053	46.25	1.382	1705.2
#P4	26.70	7.07	1.072	56.40	1.388	1720.9
#P5	29.30	5.93	1.064	45.20	1.391	1726.1
#P6	21.10	6.82	1.071	61.80	1.384	1700.2
#P7	18.70	5.94	1.062	61.45	1.380	1682.2
#P8	18.20	5.74	1.061	59.50	1.379	1680.3
#PV1	20.20	5.60	1.053	61.00	1.374	1679.8
#PV2	27.20	6.39	1.066	56.55	1.387	1716.8
#PV3	26.40	4.74	1.051	47.25	1.382	1701.1
#PV4	32.40	8.47	1.089	59.05	1.399	1754.8

C-2 Pilot plant samples

Table C-3: MEA and CO_2 concentrations and raw measurement data of the pilot samples

Operation [h]	MEA [wt% unl. solv.]	CO_2 [wt%]	Density [g/ml]	Conductivity [mS/cm]	Refr. ind. [n_D20]	Sonic speed [m/s]
12.9	32.06	5.71	1.063	32.55	1.388	1730.3
17.8	29.15	8.70	1.092	49.40	1.392	1741.0
17.8	31.23	6.17	1.065	35.15	1.386	1723.2
35.9	32.16	5.11	1.057	30.90	1.386	1720.5
436.5	35.42	10.42	1.115	43.50	1.405	1785.3
707.4	34.03	5.92	1.064	32.10	1.390	1734.2
707.4	33.96	10.45	1.108	47.85	1.400	1769.8
852.2	35.32	10.00	1.108	46.65	1.401	1772.5
852.2	35.94	6.04	1.067	31.90	1.391	1739.4
1017.1	33.92	10.12	1.109	47.45	1.401	1770.2
1017.1	33.86	5.95	1.064	31.25	1.390	1733.9

C-3 Microplant experiments

Table C-4: Measurement data used for prediction of the MEA and CO_2 concentrations in the samples taken during the continuous experiment at the microplant

Samples	MEA [wt% unl. solv.]	CO_2 [wt%]	Density [g/ml]	Conductivity [mS/cm]	Refr. ind. [n_D20]	Sonic speed [m/s]
#1	29.47	3.55	1.037	25.57	1.376	1694.7
#2	29.98	6.90	1.073	37.43	1.386	1726.0
#3	29.99	7.36	1.077	38.56	1.387	1730.7
#4	30.26	9.06	1.094	45.10	1.392	1744.1
#5	30.04	9.19	1.096	45.29	1.392	1745.8
#6	30.24	7.81	1.078	42.27	1.388	1732.2
#7	29.95	9.04	1.091	44.27	1.390	1739.3
#8	29.91	7.38	1.074	43.41	1.386	1725.9
#9	29.27	7.13	1.073	38.69	1.385	1721.2
#10	28.82	8.76	1.089	45.44	1.389	1732.9
#11	28.48	8.48	1.088	45.89	1.388	1730.1
#12	26.88	6.53	1.068	44.82	1.381	1706.7
#13	27.76	6.62	1.071	42.92	1.383	1713.7
#14	28.81	8.56	1.090	46.09	1.389	1735.7
#15	26.96	6.21	1.067	44.26	1.381	1707.7
#16	26.46	6.42	1.067	42.42	1.381	1706.3
#17	25.62	5.84	1.062	39.28	1.379	1698.1
#18	24.19	3.61	1.038	35.12	1.371	1675.4
#19	24.62	5.48	1.059	37.02	1.377	1692.7
#20	24.69	5.56	1.058	37.15	1.376	1690.4
#21	24.73	5.82	1.060	37.92	1.377	1692.7
#22	24.41	5.83	1.059	38.18	1.376	1690.1
#23	24.59	5.91	1.060	38.61	1.377	1692.0
#24	24.58	5.89	1.060	38.71	1.377	1691.5

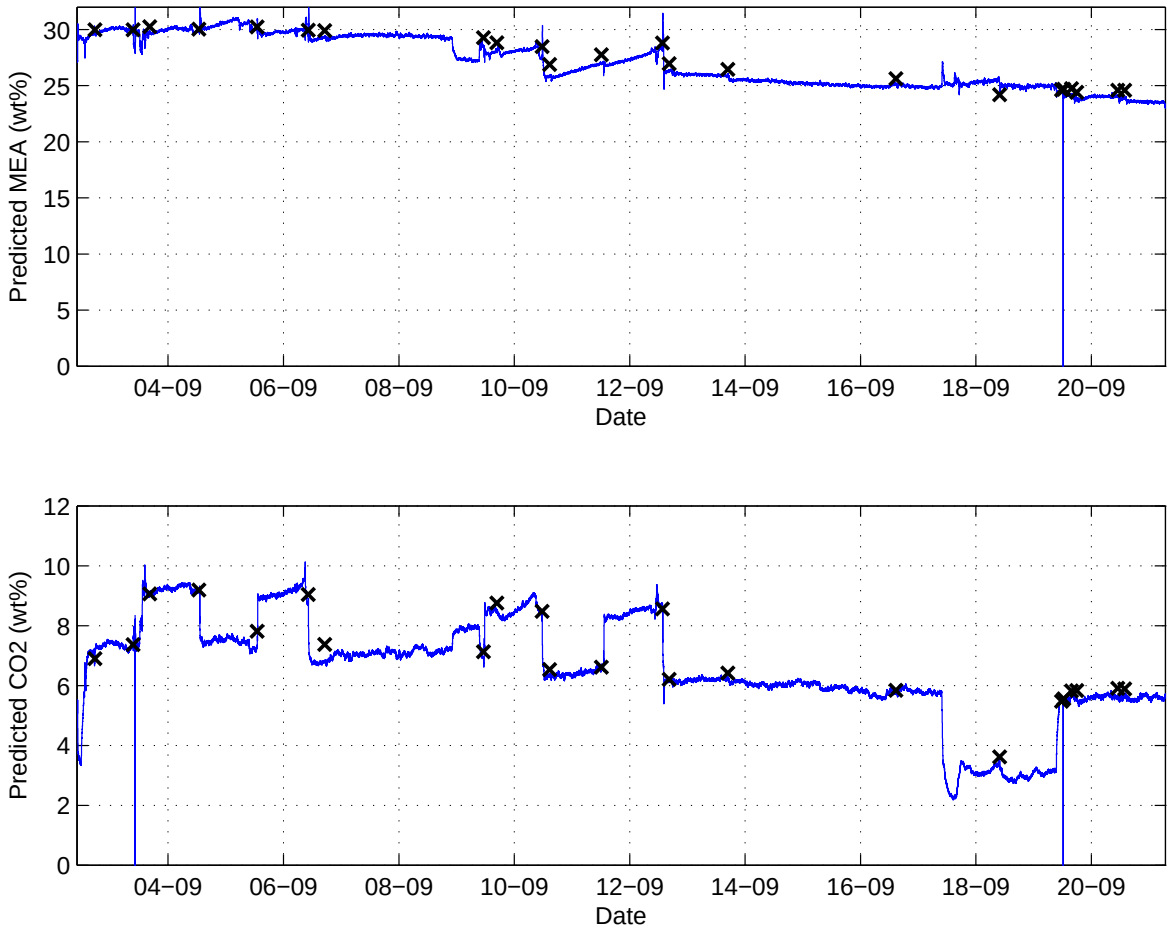

Figure C-1: Continuously predicted MEA and CO_2 concentrations and concentrations in analysed samples (marks) during the microplant experiments, obtained with the polluted model

Appendix D

D-1 VLE data

Table D-1: Coefficients used in the Oexmann equation [40]

Coefficient	Value
$C_{pCO_2,0}$	22.53
$C_{pCO_2,1}$	-7904
$C_{pCO_2,2}$	105
$C_{pCO_2,3}$	-16810
$C_{pCO_2,4}$	-286.4
$C_{pCO_2,5}$	26480
$C_{pCO_2,6}$	381.7
$C_{pCO_2,7}$	8294
$C_{pCO_2,8}$	-257.4

Fitted parameter used in Equation 6-3. Parameters were fitted to the MEA concentration using a second order polynomial fit. Values for the coefficients are listed in Table D-2.

$$A = a_1 * x_{MEA}^2 + a_2 * x_{MEA} + a_3 \tag{D-1}$$

$$B = b_1 * x_{MEA}^2 + b_2 * x_{MEA} + b_3 \tag{D-2}$$

Table D-2: Coefficients fitted to MEA concentration in Equation D-1 and D-2

Coefficient	Value
a1	-74.45
a2	15.87
a3	-2140.90
b1	-0.189
b2	-0.113
b4	7.738

Bibliography

[1] W. R. L. Anderegg, J. W. Prall, J. Harold, and S.H. Schneider. Expert credibility in climate change. In *PNAS*, volume 107, pages 12107–12109, 2010.

[2] Karl and Trenberth. Modern Global Climate Change. *Science*, 302:1719–1723, 2003.

[3] IEA. Technology Roadmap: Carbnon capture and storage. Technical report, OECD/IEA, 2013.

[4] IEA. CO_2 emissions from fuel combustion. Technical report, OECD/IEA, 2012.

[5] B. Metz and et al. IPCC Special Report on Carbon Dioxide Capture and Storage. Technical report, IPCC, 2005.

[6] GCI. The global status of CCS. Technical report, GCI, 2012.

[7] P. D. Vaidya and E. Y. Kenig. CO_2-Alkanolamine Reaction Kinetics: A Review of Recent Studies. *Chem. Eng. Technol.*, 30:1467–1474, 2007.

[8] L.F.G. Geers and et al. Development of an Online Monitoring Method of a CO_2 Capture Process. *Industrial & Engineering Chemistry Research*, 50:9175–9180, 2011.

[9] A. Einbu and et al. Online analysis of amine concentration and CO_2 loading in MEA solutions by ATR-FTIR spectroscopy. In *Energy Procedia 23*, pages 55–63, 2012.

[10] J. H. van der Lee, J. A. Swallow, and B. R. Young. CO_2 loading measurements and control in an amine absorption/stripping pilot plant. In *Proceedings of the Anual ISA Analysis Division Symposium*, pages 56–65, 2003.

[11] J. H. van der Lee, J. A. Swallow, B. R. Young, and W. Y. Svrcek. Monitoring CO_2 loading of rich and lean streams in an amine absorption/stripping pilot plant. In *Proceedings of the Anual ISA Analysis Division Symposium*, pages 220–257, 2004.

[12] Pouryousefi and Idem. New Analytical Techniques for CO_2 Capture Solvents. *Industrial & Engineering Chemistry Research*, 47:1268–1276, 2008.

[13] Brent Hawrylak, Susan E. Burke, and R. Palepu. Partial Molar Excess Volumes and Adiabatic Compressibilities of Binary Mixtures of Ethanolamines with Water. *Journal of Solution Chemistry*, 29(6):575–594, 2000.

[14] L. V. van der Ham, D. E. Bakker, L. F. G. Geers, and E. L. V. Goetheer. In-line monitoring of CO_2 absorption processes using simple analytical techniques and multivariate modelling. Accepted for publication in Chem. Eng. Technol., 2013.

[15] H. Yang, Z. Xu, M. Fan, R. Gupta, R. B. Slimane, A. E. Bland, and I. Wright. Progress in carbon dioxide separation and capture: A review. *J. Environ. Sci.*, 20:14–27, 2008.

[16] Versteeg and van Swaaij. On the kinetics between CO_2 and alkanolamines both in aqueous and non-aqueous solutions. *Chemical Engineering Science*, 43:573–585, 1988.

[17] G. T. Rochelle and et al. Research needs for CO_2 Capture from Flue Gas by Aqueous Absorption/Stripping. Technical Report DE-AF26-99FT01029, US Department of Energy - Federal Energy Technology Center, 2001.

[18] L. D. Polderman and A. B. Steel. Why MEA Solution Breaks Down in Gas Treating Service. *Oil and Gas Journal*, 54:180–183, 1955.

[19] N.V. Yazvikova, L.G. Zelenskaya, and L.V. Balyasnikova. Mechanism of Side Reactions During Removal of Carbon Dioxide from Gases by Treatment with Monoethanolamine. *Zhurnal Prikladnoi Khimii*, 48(3):674, 1955.

[20] Davis and Rochelle, Gary T. Thermal degradation of monoethanolamine at stripper conditions. In *Energy Procedia 1*, pages 327–333, 2009.

[21] A. J. Sexton. *Amine Oxidation in CO_2 capture processes.* PhD thesis, University of Texas at Austin, 2008.

[22] Supap, et al. Mechanism of Formation of Heat Stable Salts (HSSs) and their Roles in Further Degradation of Monoethanolamine during CO_2 Capture from Flue Gas Streams. In *Energy Procedia 4*, pages 591–598, 2011.

[23] K.A. Bakeev. *Process Analytical Technology.* Blackwell Publishing, 3rd edition, 2007.

[24] K. R. Beebe, R. J. Pell, and M. B. Seasholtz. *Chemometrics: A Practical Guide.* John Wiley & Sons, Inc., 6th edition, 1998.

[25] R. Kramer. *Chemometric Techniques for Quantitative Analysis.* Marcel Dekker, Inc., 4th edition, 1998.

[26] S. Wold. Chemometrics; what do we mean with it, and what do we want from it? *Chemometr. Intell. Lab. Syst.*, 30:109–115, 1995.

[27] M. Dhanoa, S. Lister, R. Sanderson, and R. Barnes. The link between Multiplicative Scatter Correction (MSC) and Standard Normal Variate (SNV) transformations of NIR spectra. *J. Near Infrared Spectrosc.*, 2:43, 1994.

[28] H. Wold. Estimation of principal components and related models by iterative least squares. *Multivariate analysis*, 1:391–420, 1966.

[29] S. de Jong. SIMPLS: an alternative approach to partial least squares regression. *Chemometr. Intell. Lab. Syst.*, 18:251–263, 1992.

[30] A. B. Rao and E. S. A. Rubin. Technical, Economic and Environmental Assessment of Amine-Based CO_2 Capture Technology for Power Plant Greehouse Gas Control. *Environ. Sci. Technol.*, 36:4467–4475, 2002.

[31] Lepaumier, et al. Comparison of MEA degradation in pilot-scale with lab-scale experiments. In *Energy Procedia 4*, pages 1652–1659, 2011.

[32] B. Fostas, A. Gangstad, B. Nenseter, S. Pedersen, M. Sjøvoll, and A. L. Sørensen. Effects of NOx in the Flue Gas Degradation of MEA. In *Energy Procedia 4*, pages 1566–1573, 2011.

[33] A. Bello and R. O. Idem. Pathways for the Formation of Products of the Oxidative Degradation of CO_2-Loaded Concentrated Aqueous Monoethanolamine Solutions during CO_2 Absorption from Flue Gases. *Ind. Eng. Chem. Res.*, 44:945–969, 2005.

[34] D. C. Montgomery. *Design and analysis of experiments.* Wiley: Hoboken, 6th edition, 2005.

[35] P. Khakharia, L. Brachert, J. Mertens, A. Huizingan, B. Schallert, K. Schaber, T. J. H. Vlugt, and E. L. V. Goetheer. Investigation of Aerosol Based Emission of MEA due to Sulphuric Acid Aerosol and Doot in a Post Combustion CO_2 Capture Process. Submitted for publication in Int. J. Greenhouse Gas Cont., 2013.

[36] S. Wold, M. Sjöström, and L. Eriksson. PLS-regression: a basic tool of chemometrics. *Chemometr. Intell. Lab. Syst.*, 58:109–130, 2001.

[37] A. Rinnan, F. van den Berg, and S. B. Engelsen. Review of the most common preprocessing techniques for near-infrared spectra. *Trends in Anal. Chem.*, 28:1201–1222, 2009.

[38] J. A. Westerhuis, S. de Jong, and A. K. Smilde. Direct Orthogonal Signal Correction. *Chemometr. Intell. Lab. Syst.*, 56:13–25, 2001.

[39] N. M. Faber and R. Bro. Standard error of prediction for multiway PLS: 1. Background and a simulation study. *Chemometr. Intell. Lab. Syst.*, 61:133–149, 2001.

[40] J. Oexmann. *Post-Combustion CO2 Capture: Energetic Evaluation of Chemical Absorption Processes in Coal-Fired Steam Power Plants.* PhD thesis, Technischen Universität Hamburg-Harburg, 2011.

[41] D. M. Austgen, G. T. Rochelle, X. Peng, and C. C. Chen. Model of Vapor-Liquid Equilibria for Aqeous Acid Gas-Alkonalamine Systems Using the Electrolyte-NRTL Equation. *Ind. Eng. Chem. Res.*, 28:1060–1073, 1989.

Glossary

List of Acronyms

CATO	CO_2 Afvang, Transport en Opslag
CCS	Carbon Capture and Storage
CLS	Classical Least Squares
FTIR	fourier transform infrared
HSS	Heat Stable Salts
IEA	International Energy Agency
IECR	Industrial & Engineering Chemistry Research
ILS	Inversed Least Squares
KIT	the Karlsruhe Institute of Technology
LVs	Latent Variables
MEA	Monoethanolamine
MSC	Multiplicative Scatter Correction
NIR	near infrared
OSC	Orthogonal Signal Correction
PCs	Principal Components
PCA	Principal Component Analysis
PCC	Post-Combustion Capture
PCR	Principal Component Regression
PLS	Partial Least Squares
PLSR	Partial Least Squares Regression
PRESS	Predicted Residual-Sum-of-Squares

RMSEC Root-Mean-Square Error of Calibration

RMSEP Root-Mean-Square Error of Prediction

SNV Standard Normal Variate

VLE Vapour Liquid Equilibrium

UV-vis visible ultra-violet

List of Symbols

Symbols

A	Absorbance spectrum
A	Fitted parameter in adapted antoine equation
B	Fitted parameter in adapted antoine equation
b	Pathlength
C	Concentration of species
c	Speed of light in a vacuum
C_{pCO_2}	Coefficients used in the Oexmann equation
d	Degrees of freedom
E	Magnitude of the electric field
E	Error matrix
J	Magnitude of the current density
K	Regression matrix
m	Mass
m	Number of samples
n	Number of variables
n	Refractive index
$\dot{n}$	Molar flow rate
$P^*_{CO_2}$	Partial pressure of CO_2 estimated using the Oexmann equation
P_{CO_2}	Partial pressure of CO_2
P	Matrix containing X-loadings
Q	Q-residual
S	Standard deviation
s	Entropy
T	Temperature
T	Scores matrix
u	Speed
V	Volume
v	Speed of light in a substance
W	Loading weights
X	Measured data
Y	Predicted data

Greek Symbols

α	CO_2 loading of the solvent
α_{cyc}	Cyclic loading
β	Ratio between actual and theoretical loading
$\boldsymbol{\lambda}$	Diagonal matrix with eigenvalues of model components

ϵ	Molar absorption coefficient
μ	Dynamic viscosity
ν	Kinematic viscosity
ρ	Density
σ	Electrical conductivity
τ	Local shear velocity

Superscripts and subscripts

^{t}	Transpose of matrix
$\widehat{}$	Estimated value
as	Autoscaled
mc	Mean centered